



HAL
open science

High turnover rates indicated by changes in the fixed N forms and their stable isotopes in Antarctic landfast sea ice

François Fripiat, Daniel M. Sigman, Guillaume Massé, Jean-Louis Tison

► To cite this version:

François Fripiat, Daniel M. Sigman, Guillaume Massé, Jean-Louis Tison. High turnover rates indicated by changes in the fixed N forms and their stable isotopes in Antarctic landfast sea ice. *Journal of Geophysical Research. Oceans*, 2015, 120 (4), pp.3079 - 3097. 10.1002/2014jc010583 . hal-01496696

HAL Id: hal-01496696

<https://hal.science/hal-01496696>

Submitted on 5 Jan 2022

HAL is a multi-disciplinary open access archive for the deposit and dissemination of scientific research documents, whether they are published or not. The documents may come from teaching and research institutions in France or abroad, or from public or private research centers.

L'archive ouverte pluridisciplinaire **HAL**, est destinée au dépôt et à la diffusion de documents scientifiques de niveau recherche, publiés ou non, émanant des établissements d'enseignement et de recherche français ou étrangers, des laboratoires publics ou privés.

Copyright

RESEARCH ARTICLE

10.1002/2014JC010583

High turnover rates indicated by changes in the fixed N forms and their stable isotopes in Antarctic landfast sea ice

François Fripiat^{1,2,3}, Daniel M. Sigman², Guillaume Massé^{4,5}, and Jean-Louis Tison¹

Key Points:

- Spring accumulation of fixed nitrogen above seawater values
- High turnover rates of fixed N pool, including nitrate
- Light availability affects sea ice nitrate isotopes distribution

Supporting Information:

- Supporting Information S1
- Supporting Information S2
- Table S1

Correspondence to:

F. Fripiat,
ffripiat@ulb.ac.be

Citation:

Fripiat, F., D. M. Sigman, G. Massé, and J.-L. Tison (2015), High turnover rates indicated by changes in the fixed N forms and their stable isotopes in Antarctic landfast sea ice, *J. Geophys. Res. Oceans*, 120, 3079–3097, doi:10.1002/2014JC010583.

Received 18 NOV 2014

Accepted 23 MAR 2015

Accepted article online 31 MAR 2015

Published online 26 APR 2015

¹Department of Earth and Environmental Sciences, Université Libre de Bruxelles, Brussels, Belgium, ²Department of Geosciences, Princeton University, Princeton, New Jersey, USA, ³Now at Analytical, Environmental and Geo-Chemistry, Earth Sciences Research Group, Vrije Universiteit Brussel, Brussels, Belgium, ⁴UMI3376 Takuvik—CNRS/Université Laval, Québec, Canada, ⁵Sorbonne Universités, UPMC, Univ Paris 06, CNRS-IRD-MNHN, LOCEAN Laboratory, Paris, France

Abstract We report concentration and nitrogen and oxygen isotopic measurements of nitrate, total dissolved nitrogen, and particulate nitrogen from Antarctic landfast sea ice, covering almost the complete seasonal cycle of sea ice growth and decay (from April to November). When sea ice forms in autumn, ice algae growth depletes nitrate and accumulates organic N within the ice. Subsequent low biological activity in winter imposes minor variations in the partitioning of fixed N. In early spring, the coupling between nitrate assimilation and brine convection at the sea ice bottom traps a large amount of fixed N within sea ice, up to 20 times higher than in the underlying seawater. At this time, remineralization and nitrification also accelerate, yielding nitrate concentrations up to 5 times higher than in seawater. Nitrate $\delta^{15}\text{N}$ and $\delta^{18}\text{O}$ are both elevated, indicating a near-balance between nitrification and nitrate assimilation. These findings require high microbially mediated turnover rates for the large fixed N pools, including nitrate. When sea ice warms in the spring, ice algae grow through the full thickness of the ice. The warming stratifies the brine network, which limits the exchange with seawater, causing the once-elevated nitrate pool to be nearly completely depleted. The nitrate isotope data point to light limitation at the base of landfast ice as a central characteristic of the environment, affecting its N cycling (e.g., allowing for nitrification) and impacting algal physiology (e.g., as reflected in the N and O isotope effects of nitrate assimilation).

1. Introduction

Sea ice is permeated by a network of brine, inhabited by a sympagic (ice-related) community that is both taxonomically diverse and metabolically active [Thomas and Dieckmann, 2002; Deming, 2010]. These communities flourish within specific microhabitats created when sea ice forms and ages [Arrigo and Thomas, 2004]. They play a significant but still poorly understood role in the biogeochemical dynamics of the polar oceans [Vancoppenolle et al., 2013], contributing to the primary production in ice-covered waters [Arrigo and Thomas, 2004], extending the productive season, and serving as the main food source for some high trophic level organisms [Flores et al., 2014, and references therein]. During sea ice growth and decay, sea ice continuously exchanges chemicals (e.g., nutrients and gases) both with the ocean and the atmosphere [Vancoppenolle et al., 2010; Lannuzel et al., 2011; Rysgaard et al., 2011; Fripiat et al., 2014]. Upon sea ice melting, the release of stored biomass and nutrients has been suggested to seed and/or fertilize the ice edge bloom [Smith and Nelson, 1985; Lancelot et al., 2009; Galindo et al., 2014]. Still, little is known about the fate of sea ice-produced organic matter. It is uncertain whether this organic matter is preferentially respired within sea ice or in the surface waters after melting or is exported to the deep ocean or seafloor.

Nitrogen (N) is required in large quantities by all organisms, and it is one of the most important nutrients for autotrophic growth. Several studies have reported evidence of an active microbial nitrogen cycle within sea ice: large variations in dissolved inorganic N concentration [Thomas et al., 2010]; rapid N assimilation (up to $80 \mu\text{mol L}^{-1} \text{h}^{-1}$) [Harrison et al., 1990]; high and variable concentrations of dissolved organic nitrogen (with estimated concentrations within the brine of up to 2.2mmol L^{-1}) [Thomas et al., 2001]; rapid turnover of the protein pool (2.7 h) [Guglielmo et al., 2000]; large contributions of nitrification to nitrate assimilation (up to 70%) [Fripiat et al., 2014]; and denitrification in oxygen-depleted microhabitats [Rysgaard et al., 2008]. The timing and the contribution of these processes to the overall sea ice N cycle remain elusive. First, the sparseness of observations renders difficult any clear mechanistic understanding of the seasonality of the

dominant processes. Second, there are inherent difficulties in manipulating sea ice microorganisms (e.g., in incubations) or in measuring the rate of a targeted metabolism (e.g., N assimilation, nitrification) [Miller *et al.*, 2015]. Third, the patchiness of sea ice physical, chemical, and biological properties implies that it is difficult to compare several adjacent ice cores where parallel experiments are conducted [Eicken *et al.*, 1991]. It appears, therefore, crucial to develop new noninvasive tracers.

The variations in the nitrogen and oxygen isotopic composition of various fixed N forms can provide an integrative picture of the N cycle, from which physical, chemical, and biochemical fluxes can be inferred ($\delta^{15}\text{N}$, in ‰ versus atmospheric N_2 ; $\delta^{18}\text{O}$, in ‰ versus Vienna Standard Mean Ocean Water) [DiFiore *et al.*, 2006, 2009; Sigman *et al.*, 2005; Wankel *et al.*, 2007; Granger *et al.*, 2013]. Most of the N transformations involve a measurable and often distinct isotopic discrimination of the N and O isotopes [Sigman *et al.*, 2009a]. The degree of fractionation is quantified as an isotope effect, which is a measure of the ratio of the reaction rates at which the isotopes are converted from one form to another (i.e., ϵ (‰) = $(^{14}\text{k}/^{15}\text{k} - 1) * 1000$ for N and $(^{16}\text{k}/^{18}\text{k} - 1) * 1000$ for O; where ^nk is the rate coefficient for the ^nN or ^nO -containing reactant) [Sigman *et al.*, 2009a]. In spring Antarctic pack ice, Fripiat *et al.* [2014] investigated the N isotopes to evaluate the overall seasonal N dynamics.

Antarctic landfast sea ice, fastened to the coastline, is one of the most productive environments on Earth (with chl-*a* concentration up to $>10,000 \mu\text{g L}^{-1}$) [Arrigo *et al.*, 1995]. Unlike Antarctic pack ice, in which biomass is relatively evenly distributed through the full thickness of the ice [Meiners *et al.*, 2012], biomass in Antarctic landfast sea ice is mainly concentrated in the bottom 20 cm [Arrigo and Thomas, 2004]. This study reports for the first time the concentrations and isotopic compositions of nitrate (NO_3^-), total dissolved N (TDN), and particulate N (PN) in Antarctic landfast sea ice (Terre Adélie, French Antarctic station "Dumont d'Urville") from April to November, covering a nearly complete fall to spring progression. The data indicate: (i) an autumnal bloom when sea ice forms, (ii) little biological activity in the wintertime, (iii) a highly productive early spring system in the bottom consolidated platelet layer, nutrient input from seawater as well rapid recycling among the different fixed N forms, including between nitrate and reduced N forms, (iv) and net NO_3^- depletion throughout the entire ice thickness due to assimilation coincident with the stratification of the brine network in later spring. The nitrate $\delta^{15}\text{N}$ and $\delta^{18}\text{O}$ throughout the spring and their depth structure during the later nitrate drawdown period suggest light limitation of nitrate assimilation near the base of the ice.

2. Materials and Methods

2.1. Sample Collection

Landfast sea ice samples were collected at two stations, located close to the Dumont d'Urville French station (Figure 1a): one in April 2011 enclosed in the "Géologie Archipelago" ($66^\circ40.159\text{S}$; $140^\circ00.143\text{E}$) and one from June to November 2011 west of the Géologie Archipelago ($66^\circ39.911\text{S}$; $139^\circ59.534\text{E}$). Sea ice appeared at the second station only in May 2011 and therefore cannot be sampled in April. The second station was more representative of the East Antarctic landfast sea ice [Fraser *et al.*, 2012].

Ice cores ($n = 10$) were collected at regular time intervals (approximately 1 month from April to September and 2 weeks from September to November) in a selected area ($100 \text{ m} \times 100 \text{ m}$). Cores were collected using a 14 cm diameter stainless-steel corer and were processed the same day in the shore-based laboratory of the Dumont d'Urville station. From each core, four ice slices (10 cm thick) were cut with a band saw and melted directly at room temperature in the dark (one at the bottom, two in the middle, and one at the surface). The samples were immediately filtered through precombusted Whatman GF/F filters. At each station, about 0.75 L of seawater was sampled through the ice core hole with a prerinsed polypropylene syringe and polycarbonate tube. An accumulation of ice platelet was observed inside the hole from September to November. Such accumulation suggests that, from September to November, we sampled either (i) the interstitial water from the loose platelet layer or (ii) a mixture of underlying seawater and interstitial water [Günther *et al.*, 1999]. Water samples were also filtered through precombusted Whatman GF/F filters in the shore-based lab. Filtered water samples were stored in 60 mL acid-washed, prerinsed polyethylene bottles at -25°C . Filters were also stored at -25°C .

Despite the fact that we have paid attention to study a level ice floe with a homogeneous surface and sample small contiguous area, we must acknowledge that a time series such as this one may be affected by

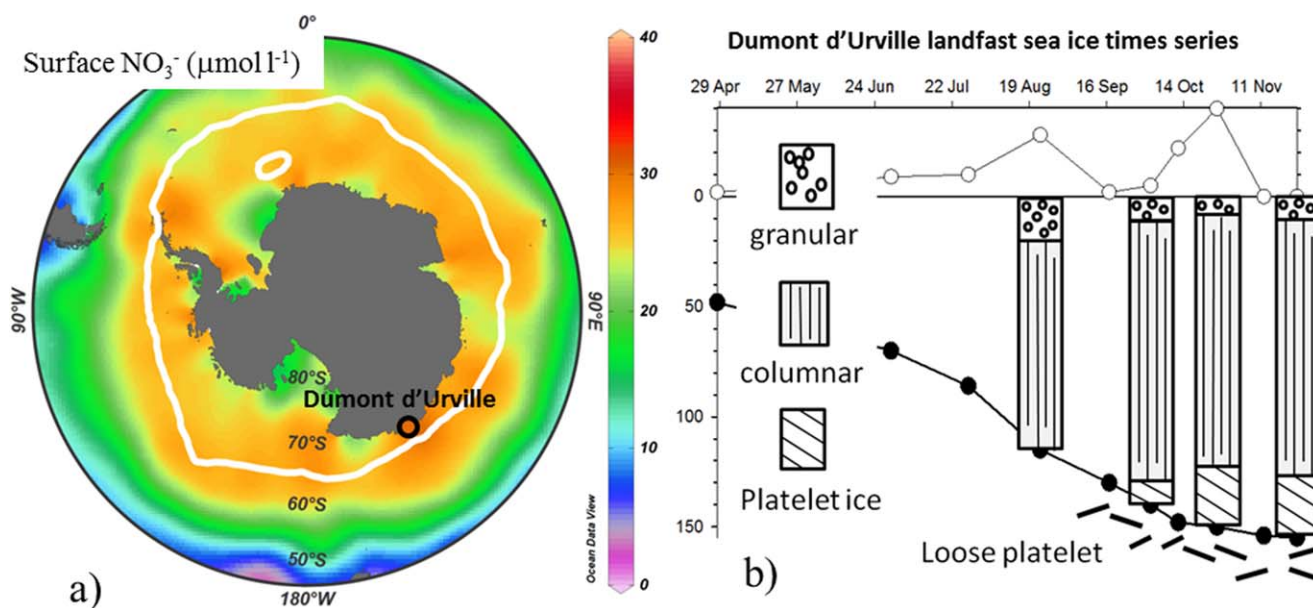


Figure 1. (a) Circumpolar view of the mean annual surface nitrate concentration, from the World Ocean Atlas climatology 2005 [Garcia et al., 2005], combined with the delineation (white line) of September sea ice extent (with sea ice cover representing >50% of the specific area). Interpolation and sea ice extent is from Ocean Data View [Schlitzer, 2015]. The sea ice time series station, in the vicinity of French station "Dumont d'Urville," is represented with the colored circle, and its color corresponds with the seawater nitrate concentration reported in this study. (b) Temporal evolution of the sea ice properties, with ice depth (cm; black circles), snow depth (cm; white circles), and ice textures. The first station enclosed in the "Géologie Archipelago" was sampled only in April, when open-water conditions prevailed at the second station. From June to November, the second station west of the Géologie Archipelago was sampled.

spatial variability that could not be completely assessed when we discuss the evolution of biogeochemical processes [Tison et al., 2008]. Accordingly, we focus on the large variations in the concentrations and isotopes of fixed N, such as occur during the winter-spring transition and in the bloom at the bottom consolidated platelet layer in October.

2.2. Nitrogen Analyses

The concentration of nitrate plus nitrite was measured by reduction to nitric oxide (NO) in a hot (95°C), acidic vanadium (III) solution, followed by chemiluminescence detection of NO [Braman and Hendrix, 1989] using a Teledyne 200E chemiluminescence NOx analyzer (Thousand Oaks, CA, USA). Nitrite concentration was measured by reduction to NO in a hot (95°C) acidic iodine solution also followed by chemiluminescence detection [Garside, 1982]. From the measured concentrations of nitrate plus nitrite and nitrite only, the concentration of nitrate only was calculated by subtraction. Ammonium concentration was measured using the fluorometric method of Holmes et al. [1999].

Prior to nitrate isotope analysis, nitrite was removed with the sulfamic acid protocol of Granger and Sigman [2009]. The $\delta^{15}\text{N}$ and $\delta^{18}\text{O}$ of nitrate were measured using the "denitrifier method" [Sigman et al., 2001; Casciotti et al., 2002]. Measurements were referenced to air N_2 and VSMOW using the nitrate reference materials IAEA-N3, with a $\delta^{15}\text{N}$ of 4.7‰ and a $\delta^{18}\text{O}$ of 25.6‰, and USGS-34, with a $\delta^{15}\text{N}$ of -1.8‰ and a $\delta^{18}\text{O}$ of -27.9‰ [Böhlke et al., 2003]. Twenty-five percent of our samples had a NO_3^- concentration lower than 3 $\mu\text{mol l}^{-1}$ (minimum NO_3^- concentration = 0.37 $\mu\text{mol l}^{-1}$). For these samples, we applied the evaporative technique described in Fripiat et al. [2014]. Replicate analyses (100% of the samples) indicate an average 1 sd reproducibility of 0.05‰ and 0.23‰ ($n = 57$) for the nitrate $\delta^{15}\text{N}$ and $\delta^{18}\text{O}$, respectively, including evaporated samples.

The concentration and $\delta^{15}\text{N}$ of total dissolved nitrogen ($\text{TDN} = \text{NO}_3^- + \text{NO}_2^- + \text{NH}_4^+ + \text{DON}$) and a fraction of filters dedicated to particulate nitrogen (PN; $n = 37$) were determined using the coupled persulfate oxidation/denitrifier method of Knapp et al. [2005], which involves the oxidation of reduced fixed N species to nitrate, followed by the analysis of the concentration and $\delta^{15}\text{N}$ of the resultant nitrate using the chemiluminescence and denitrifier methods described above. To correct for the blank associated with the persulfate oxidizing reagent (POR), triplicates of different amounts (15 and 60 nmol N) of two L-glutamic acid reference materials (USGS-40, with a $\delta^{15}\text{N}$ of -4.5‰, and USGS-41, with a $\delta^{15}\text{N}$ of 47.6‰) [Qi et al., 2003] were

processed along with the samples. Replicate analyses (100% of the samples) indicate an average 1 sd reproducibility of 0.09‰ and 0.22‰ ($n = 57$ and 37) for TDN and PN $\delta^{15}\text{N}$, respectively. For the samples with large quantities of biomass ($n = 12$), particulate nitrogen analyses were performed on a DeltaV IRMS coupled to a Costech CHNSO Elemental Analyzer via a ConFlo IV interface. GF/F filters were packed into silver envelopes and flash combusted at $\sim 1400^\circ\text{C}$. Isotopic composition was calibrated using an in-house standard (Aminocaproic acid, $\delta^{15}\text{N} = 3.9 \pm 0.1\text{‰}$). Replicate analyses (100% of the samples) indicate an average 1 sd reproducibility of 0.21‰ ($n = 12$) for the PN $\delta^{15}\text{N}$. By measuring NO_3^- and TDN $\delta^{15}\text{N}$, we calculate the $\delta^{15}\text{N}$ of the remaining dissolved fixed nitrogen, which includes dissolved organic nitrogen (DON), ammonium (NH_4^+) and nitrite (NO_2^-). The median contribution of NO_2^- to the $\text{DON} + \text{NH}_4^+ + \text{NO}_2^-$ was 0.6% (with 3% being the highest observed); hereafter, this pool is referred to as $\text{DON} + \text{NH}_4^+$ only.

3. Results

3.1. Physical Framework

Ice thickness increased during the sampling period (from 45 to 154 cm), with variable snow cover (0–40 cm; Figure 1b). Ice texture was, from top to bottom: granular ice, columnar ice, and consolidated platelet ice (Figure 1b). Consolidated platelet ice was observed from 2 October until the end of the experiment, with the columnar/platelet boundary at 122 ± 9 cm. An accumulation of loose ice platelets was observed at the bottom of the ice floe in September, as commonly observed in this area (Figure 1b) [e.g., *Riaux-Gobin et al.*, 2005; *Delille et al.*, 2007]. These platelet ice crystals are produced from super-cooled water, advected from underneath the ice shelves, and progressively incorporated into the overlying sea ice cover by freezing in the interstices to form the consolidated platelet layer [e.g., *Dempsey and Langhorne*, 2012].

Figure 2 shows the evolution of temperature, brine salinity, and brine volume fraction [following *Cox and Weeks*, 1983]. Ice temperature decreased upward from the freezing temperature at the seawater interface (Figure 2a). The temperature gradients were much steeper during the winter months, with near-surface temperature reaching as low as -18.4°C . At the end of the experiment, the temperature profile was nearly isothermal, reaching only as low as -3.2°C . Brine salinity, as derived from temperature profiles based on the assumption of thermodynamic equilibrium [Cox and Weeks, 1983], decreased downward from as high as 273 down to 30 g kg^{-1} , close to local seawater values of 33 g kg^{-1} (Figure 2b). The difference between the top and the bottom layers was greatly diminished in spring, decreasing downward from 63 to 30 g kg^{-1} . Brine volumes ranged from 2.2 to 17.2%, with the lower volumes associated with the colder temperatures of the winter months (Figure 2c). Except for the last three profiles (from 26 October to 24 November), only the bottom ice layer had a brine volume fraction above 5% (Figure 2c), which is considered to be a permeability threshold for fluid transport through sea ice [e.g., *Golden et al.*, 1998; *Petrich et al.*, 2006]. Anomalous low brine volumes in the bottom layer in 28 July and 12 November may have been due to some brine loss on core sampling [Notz et al., 2005] or to small spatial variability in the desalination processes across our sampling location.

3.2. Fixed N Partitioning, $\delta^{15}\text{N}$ and $\delta^{18}\text{O}$

3.2.1. Underlying Seawater

The underlying seawater in the winter (from April to August) possessed NO_3^- concentration, $\text{NO}_3^- \delta^{15}\text{N}$ and $\text{NO}_3^- \delta^{18}\text{O}$ of $29.9 \pm 1.5 \mu\text{mol L}^{-1}$, $5.0 \pm 0.1\text{‰}$, and $2.4 \pm 0.3\text{‰}$, respectively (Figures 3 and 4), similar to those previously encountered in the Polar Antarctic Zone winter mixed layer [DiFiore et al., 2009]. However, unlike what is expected for the winter mixed layer, high concentrations and $\delta^{15}\text{N}$ were observed for $\text{DON} + \text{NH}_4^+$ ($20.2 \pm 1.2 \mu\text{mol L}^{-1}$ and $10.0 \pm 1.5\text{‰}$) and PN ($3.1 \pm 0.5 \mu\text{mol L}^{-1}$ and $8.7 \pm 1.1\text{‰}$).

3.2.2. Loose Platelet Layer (i.e., Interstitial Waters)

From 17 September, an accumulation of loose platelet ice crystals occurred at the bottom of the ice (Figure 1b). From that time forward, instead of sampling underlying seawater, we sampled either (i) the interstitial water from the loose platelet layer (ii) or a mixture of underlying seawater and interstitial water [Günther et al., 1999]. In the following discussion, this is referred to as the interstitial water. From September to the end of October, this interstitial water had NO_3^- concentration, $\delta^{15}\text{N}$, and $\delta^{18}\text{O}$ similar to that of seawater (Figures 3 and 4). In November, NO_3^- was depleted (down to $0.7 \mu\text{mol L}^{-1}$), and, as expected from the preferential assimilation of ^{14}N - and ^{16}O -bearing nitrate, $\text{NO}_3^- \delta^{15}\text{N}$ and $\delta^{18}\text{O}$ increased (up to 17.5 and 21.3‰, respectively). PN concentration steadily increased in the loose platelet layer from September to November

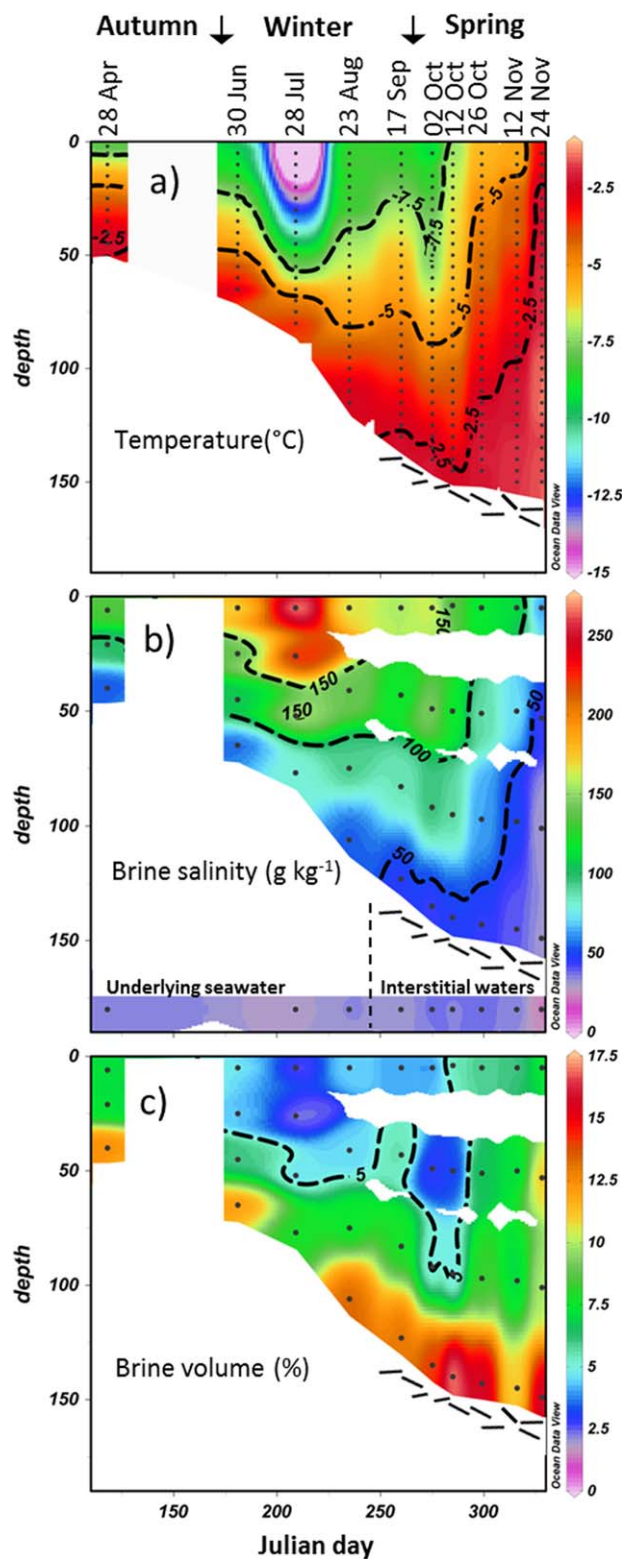


Figure 2. (a) Ice temperature, (b) brine salinity, and (c) brine volume computed assuming brine thermodynamic equilibrium [Cox and Weeks, 1983]. In Figure 2b, seawater and/or loose platelet interstitial water salinities are shown in the lower colored band of the section. Dots indicate a sampling depth. Interpolation is from Ocean Data View [Schlitzer, 2015]. The reader should be wary of extrapolated color contours.

(from 17.7 to 51.3 $\mu\text{mol L}^{-1}$; Figure 3d). This concentration should probably be taken as an underestimate since a significant fraction of the PN was likely attached to the ice platelets and therefore not sampled [Dieckmann *et al.*, 1992; Günther *et al.*, 1999]. PN $\delta^{15}\text{N}$ decreased significantly (to $4.9 \pm 0.6\text{‰}$) concurrently with the accumulation of platelet ice (Figure 4d). At the same time, the concentration of $\text{DON} + \text{NH}_4^+$ increased (to $27.2 \pm 14 \mu\text{mol L}^{-1}$) and its $\delta^{15}\text{N}$ decreased (to $7.6 \pm 1.7\text{‰}$) (Figures 3e and 4e).

3.2.3. Sea Ice

As with the salinity of sea ice brine, its nutrient distribution changes due to temperature-induced dilution or concentration during melting and freezing processes within the sea ice. To correct for these effects, all concentrations were normalized to the salinity of underlying seawater (normalized concentration = SI concentration * SW salinity/SI salinity, where SI is sea ice and SW is underlying seawater).

During the winter months (June–August), salinity-normalized NO_3^- concentration in sea ice is not significantly different from that of the underlying seawater ($26.8 \pm 3.1 \mu\text{mol L}^{-1}$ versus $29.9 \pm 1.5 \mu\text{mol L}^{-1}$, respectively; Figure 3a), with both NO_3^- $\delta^{15}\text{N}$ and $\delta^{18}\text{O}$ slightly higher in the sea ice ($5.6 \pm 0.3\text{‰}$ and $3.3 \pm 0.4\text{‰}$, respectively; Figures 4a and 4b). Except in the bottom layers in October, NO_3^- was depleted during the spring months (September–November; down to $3.6 \mu\text{mol L}^{-1}$), as usually observed in sea ice with the accumulation of biomass and its associated NO_3^- assimilation [e.g., Gleitz *et al.*, 1995]. Such depletion was stronger and occurred earlier in the internal parts of the ice floe. Associated with NO_3^- depletion, NO_3^- $\delta^{15}\text{N}$ and $\delta^{18}\text{O}$ became progressively higher (Figures 3a, 4a, and 4b). A strong accumulation of NO_3^- was observed at the bottom of the ice in October, with a salinity-normalized

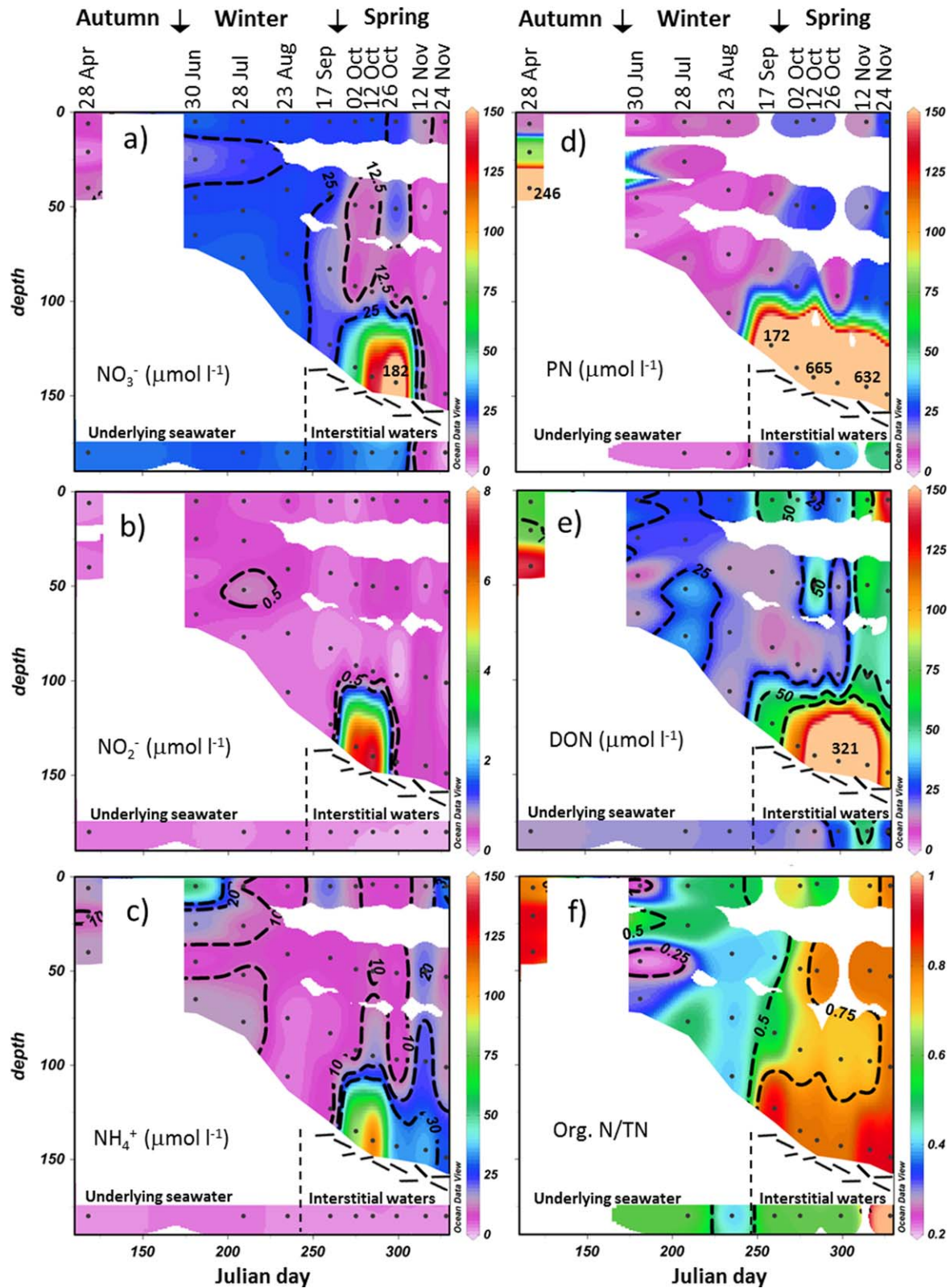


Figure 3. Salinity-normalized concentration of (a) NO_3^- , (b) NO_2^- , (c) NH_4^+ , (d) PN, (e) DON, and (f) the ratio of organic N versus total fixed N. Seawater and loose platelet interstitial water concentrations are shown in the lower colored band of the section. For the sake of clarity, only a subset of the NO_3^- , PN, and DON values above $150 \mu\text{mol N L}^{-1}$ (a, d, e) in the bottom community in October are indicated with printed values. The readers can find these values in Figure 5a. Interpolation is from Ocean Data View [Schlitzer, 2015]. The reader should be wary of extrapolated color contours.

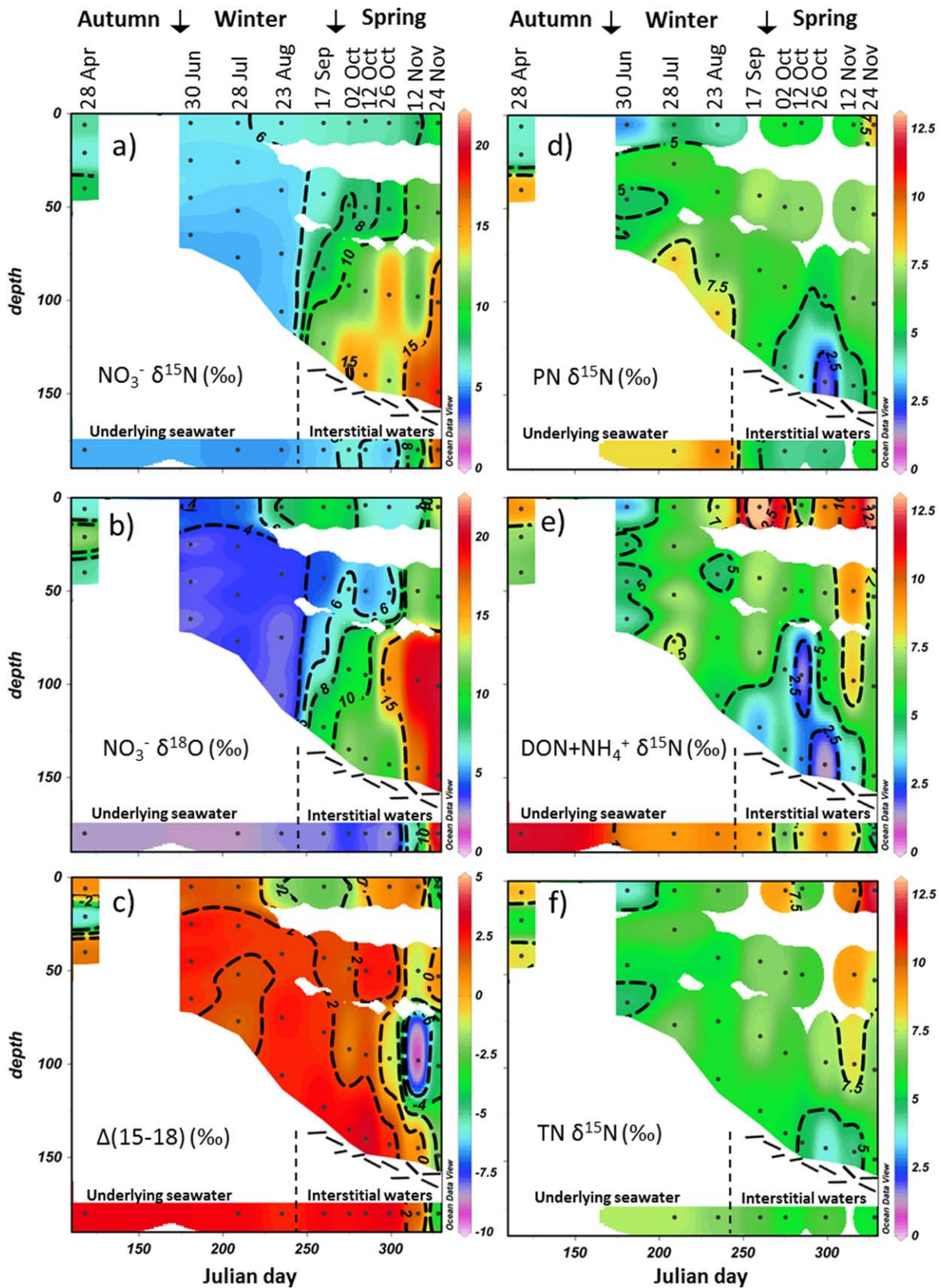


Figure 4. (a) $\text{NO}_3^- \delta^{15}\text{N}$, (b) $\text{NO}_3^- \delta^{18}\text{O}$, (c) $\Delta(15-18)$, (d) PN $\delta^{15}\text{N}$, (e) $\text{DON} + \text{NH}_4^+ \delta^{15}\text{N}$, and (f) TN $\delta^{15}\text{N}$. Seawater and loose platelet interstitial water isotopic composition are shown in the lower colored band of the section. Interpolation is from Ocean Data View [Schlitzer, 2015]. The reader should be wary of extrapolated color contours.

concentration of up to $182.3 \mu\text{mol L}^{-1}$. This nitrate had high $\delta^{15}\text{N}$ and $\delta^{18}\text{O}$ (up to 15.2‰ and 12.3‰ , respectively). Except at the bottom of the consolidated platelet layer in spring where an accumulation occurred, salinity-normalized NO_2^- concentration remained low (usually below $0.5 \mu\text{mol L}^{-1}$; Figure 3b), with a median contribution to the $\text{NO}_3^- + \text{NO}_2^-$ pool of 1%.

During the winter months (June–August), salinity-normalized $\text{DON} + \text{NH}_4^+$ concentration was slightly higher in sea ice ($34.7 \pm 18.4 \mu\text{mol L}^{-1}$) than in the underlying seawater ($20.2 \pm 1.2 \mu\text{mol L}^{-1}$; Figure 3e), but not significantly different. During this period, ammonium contributed more to the $\text{DON} + \text{NH}_4^+$ pool ($32 \pm 17\%$) than in seawater ($13 \pm 5\%$). $\text{DON} + \text{NH}_4^+$ $\delta^{15}\text{N}$ was lower ($5.6 \pm 1.6\text{‰}$) than in seawater ($10.0 \pm 1.5\text{‰}$; Figure 4e). In springtime, an accumulation of $\text{DON} + \text{NH}_4^+$ was observed at all depths (Figure 3e), with higher normalized $\text{DON} + \text{NH}_4^+$ concentration in the bottom layer (up to $353.6 \mu\text{mol L}^{-1}$), intermediate in the top layer (up to $175.8 \mu\text{mol L}^{-1}$), and lower in the intermediate layers (up to $85.6 \mu\text{mol L}^{-1}$). Ammonium contributed $26 \pm 12\%$ of the $\text{DON} + \text{NH}_4^+$ pool, with no significant depth variation. $\text{DON} + \text{NH}_4^+$ $\delta^{15}\text{N}$ evolved differently at different ice depths from winter to spring, increasing in the surface and internal layers (to 13.5‰ and 9.3‰ , respectively) and decreasing in the bottom layer (to 1.1‰ ; Figure 4e). A large Adélie penguin population in the Géologie Archipelago is the likely source of the high- $\delta^{15}\text{N}$ organic N and NH_4^+ in the upper (and possibly also intermediate) ice levels [Wada *et al.*, 1981; Thomas, 1986]. Penguin activity and wind transport of organic N from ornithogenic soils could deposit organic N on the top of sea ice, become processed into $\text{DON} + \text{NH}_4^+$ through bacterial activity (if the N was not already in this form), and exchanged with the internal layers upon the opening of the brine network in spring (Figure 2c). This high- $\delta^{15}\text{N}$ additional input was also translated into the total fixed nitrogen $\delta^{15}\text{N}$, showing a significant increase in the upper and intermediate ice levels in spring (Figure 4f). For the sake of brevity, the springtime $\text{DON} + \text{NH}_4^+$ accumulation in the surface and internal layers will not be discussed in detail below.

During the winter months, normalized PN concentration was higher in sea ice ($6.6 \pm 4.0 \mu\text{mol L}^{-1}$) than in seawater ($3.1 \pm 0.5 \mu\text{mol L}^{-1}$; Figure 3d), but not significantly different. The concentrations of PN in both the sea ice and the underlying seawater are significantly greater than is typically encountered in the open Antarctic surface waters [Martiny *et al.*, 2013] (again probably related to the ornithogenic effects; see below). PN $\delta^{15}\text{N}$ during winter was lower ($5.7 \pm 1.7\text{‰}$) than in underlying seawater ($8.7 \pm 1.1\text{‰}$; Figure 4e) and was indistinguishable from $\text{DON} + \text{NH}_4^+$ $\delta^{15}\text{N}$. In the springtime, an accumulation of PN was observed, in agreement with the concomitant NO_3^- depletion, with higher normalized PN concentration in the bottom layer (up to $664.9 \mu\text{mol L}^{-1}$) than in the intermediate and top layers (up to $29.9 \mu\text{mol L}^{-1}$; Figure 3d). For both the surface and internal layers, no significant difference from winter was observed for PN $\delta^{15}\text{N}$ ($6.5 \pm 1.0\text{‰}$), with the exception of the 24 November surface layer harboring a higher PN $\delta^{15}\text{N}$ of 8.5‰ (Figure 4d). As for $\text{DON} + \text{NH}_4^+$, PN $\delta^{15}\text{N}$ in the bottom layer decreased first (down to 1.6‰ on 26 October) and then increased again (up to 5.2‰ on 24 November).

4. Discussion

Antarctic landfast sea ice is one of the most productive environments on Earth [Arrigo and Thomas, 2004]. Most of the biomass is concentrated in the bottom centimeters in spring (e.g., Figure 3d), providing a habitat that is both stable and continuously supplied with seawater-borne nutrients [Vancoppenolle *et al.*, 2013]. The following discussion will begin with an identification of sources, as well as the modifications, of fixed N in the brine inclusions in winter. Then, the N biogeochemical dynamics of the bottom sea ice algal bloom will be discussed, followed by the decline of the bloom in November. Our focus on the bottom ice community is motivated by its dominance in terms of fixed N quantities (Figure 3) and by its importance for polar ocean biogeochemistry on a broad scale, in part because of its exchanges with the underlying water. Moreover, as described above, the upper surface of the ice is influenced by penguin-derived nitrogen, which is interesting but of narrower import, and thus we do not pursue it further here. The middepths of the ice involve relatively low concentrations of fixed N, such that the N cycle at these depths is significantly influenced by both shallower and deeper ice processes; accordingly, while the internal ice was a major focus of our pack ice studies [Fripiat *et al.*, 2007, 2014], it is secondary to the ice base in our discussion of the landfast ice data below.

4.1. Sources and Modification of Sea Ice Fixed N in Winter

Sea ice forms from the freezing of seawater. The salt trapped within sea ice is efficiently excluded from the ice crystals [Weeks and Ackley, 1986], remaining dissolved in liquid inclusions of saline brine [e.g.,

Vancoppenolle *et al.*, 2010]. Seawater represents the main source of fixed N within sea ice. Assuming the underlying seawater as representative of this source, we calculate the sea ice initial total N (TN = PN + TDN) concentration and $\delta^{15}\text{N}$ to be $52.3 \pm 2.3 \mu\text{mol L}^{-1}$ and $7.1 \pm 0.5\text{‰}$, respectively (Figure 4f for TN $\delta^{15}\text{N}$). This is significantly higher than estimated by Fripiat *et al.* [2014] for the pack ice in the polar Antarctic zone ($35 \mu\text{mol L}^{-1}$ and 4.9‰ , respectively). This difference is largely due to much higher DON + NH_4^+ concentration ($20.2 \pm 1.2 \mu\text{mol L}^{-1}$) and $\delta^{15}\text{N}$ ($10.0 \pm 1.5\text{‰}$; Figures 3 and 4). As mentioned above, from the end of October to March, a large Adélie penguin population (more than 60,000 individuals) is observed at the Géologie Archipelago [Thomas, 1986]. Large rookeries produce a substantial amount of organic matter, influencing the biogeochemistry in the surrounding coastal waters [Delille, 1990] and elevating the $\delta^{15}\text{N}$ of the local N cycle [Wada *et al.*, 1981]. The proposed mechanism for such high $\delta^{15}\text{N}$ is that the soils microorganisms convert organic nitrogen to ammonium(a), the partial volatilization of which raises the residual N $\delta^{15}\text{N}$ [Wada *et al.*, 1981]. The remaining high $\delta^{15}\text{N}$ can be transferred to the surrounding waters, explaining the observed high DON + NH_4^+ concentration and $\delta^{15}\text{N}$ in the local seawater (Figures 3 and 4).

In winter, only at the interface with the ocean, where sea ice is permeable, can fixed N be exchanged with underlying seawater. At the surface and in the interior of the ice, the brine volume fraction is too low to allow brine convection, despite the potential energy for convection from the high brine salinity (Figure 2) [Griewank and Notz, 2013]. These brine structures are closed, with fixed N concentration mainly inherited from the underlying seawater. During the winter months (June to August), salinity-normalized concentrations of the different dissolved N forms were not different, although more variable, than in local seawater (Figure 3). This lack of coherent change is explained by the low overall biological activity in the winter ice, resulting from environmental conditions not favorable for biological growth: low light (down to $0.01 \text{ kJ cm}^{-2} \text{ d}^{-1}$) [Delille *et al.*, 2002], low temperature (down to -18.4°C), and high brine salinity (up to 273 g kg^{-1} ; Figure 2).

As an exception, high salinity-normalized NH_4^+ concentration was observed at the surface of the ice in June (Figure 3c). Measurements from the first station (sampled only in April when open-water conditions still prevailed at the second station) provide evidence of a sea ice algal bloom in autumn: NO_3^- depletion in the ice, and accumulation of PN, DON, and NH_4^+ (Figure 3) [Gleitz *et al.*, 1995]. Such algal blooms have been observed previously in this area [Delille *et al.*, 2002]. The NH_4^+ accumulation in the surface layer in June likely represented the degradation product of such a bloom. The absence of a similar accumulation of ammonium in the subsequent cores may also be due to small spatial scale variability in the autumn sea ice algal bloom.

Winter sea ice NO_3^- $\delta^{15}\text{N}$ and $\delta^{18}\text{O}$ were slightly higher than in seawater, and reduced N $\delta^{15}\text{N}$ (DON, PN, and NH_4^+) was lower than in seawater (Figure 4). Such partitioning of N and O isotopes between the different fixed N forms suggests that a modest amount of NO_3^- assimilation had occurred. When NO_3^- assimilation proceeds, ^{14}N and ^{16}O isotopes are preferentially assimilated, increasing the residual NO_3^- $\delta^{15}\text{N}$ and $\delta^{18}\text{O}$ [Granger *et al.*, 2004, 2010] and decreasing the organic N $\delta^{15}\text{N}$. The similarity between the DON + NH_4^+ and PN $\delta^{15}\text{N}$ suggests that a significant fraction of this newly produced PN was converted into DON + NH_4^+ , with either DON release (PN \rightarrow DON) and/or ammonification (PN, DON \rightarrow NH_4^+). Cell damage and viral infection with the onset of the extreme winter conditions should, indeed, promote the release of DON [Günther *et al.*, 1999], and some heterotrophic bacterial activity has been observed in winter sea ice at temperatures as low as -20°C [Junge *et al.*, 2004]. Field and laboratory studies suggest that both bacteria and zooplankton preferentially degrade low- $\delta^{15}\text{N}$ PN to ammonium, with a net isotope effect of $\sim 2\text{--}5\text{‰}$ [e.g., Checkley and Miller, 1989; Knapp *et al.*, 2011; Möbius, 2013, and references therein]. Ammonification is likely the main N isotope-discriminating step in this remineralization process, breaking a N-containing bond. Little or no isotopic discrimination is expected with the production of DON, since this process only occasionally involves the breaking of N-containing bonds and then only a small fraction of the total N-containing bonds in the organic matter being processed [e.g., Knapp *et al.*, 2011, and references therein]. Production of DON + NH_4^+ without similar rates of assimilation or oxidation of the NH_4^+ can thus explain the $\delta^{15}\text{N}$ similarity between DON + NH_4^+ and PN. Both NH_4^+ assimilation and oxidation fractionate the N isotopes [Casciotti *et al.*, 2003; Vo *et al.*, 2013], such that significant rates of the ammonium-consuming processes would elevate the $\delta^{15}\text{N}$ of DON + NH_4^+ . The isotopic discrimination associated with the ammonification of DON to NH_4^+ will not affect the $\delta^{15}\text{N}$ of the combined DON + NH_4^+ pool. Ammonification of PN to NH_4^+ will increase PN $\delta^{15}\text{N}$, but the resulting high $\delta^{15}\text{N}$ will be, then, transmitted to the DON upon DON release from the PN, further dampening the isotopic difference between PN and DON + NH_4^+ .

4.2. Sea Ice Algal Bloom in the Bottom Platelet Layers

Platelet ice crystals are produced from supercooled water advected from underneath the ice shelves and accumulated at the bottom of the ice, producing a loose platelet layer first observed in our sampling area in September. Over time, the upper portion of this layer was incorporated into the overlying sea ice cover by freezing of the interstices, producing a consolidated platelet layer of ~ 20 cm thick in the sampling area between September and November (Figure 1b) [e.g., *Dempsey and Langhorne*, 2012]. A large accumulation of fixed N (up to $1127 \mu\text{mol L}^{-1}$) was observed in the consolidated platelet layer in October, ~ 30 times higher than Antarctic seawater values, with salinity-normalized concentrations of PN up to $665 \mu\text{mol L}^{-1}$, DON up to $321 \mu\text{mol L}^{-1}$, NO_3^- up to $182 \mu\text{mol L}^{-1}$, and NH_4^+ up to $115 \mu\text{mol L}^{-1}$ (Figures 3 and 5a). In the loose platelet layer below, biomass increased steadily from September to October but appeared to have only a marginal impact on NO_3^- concentration until November when NO_3^- started to become depleted (Figure 3a; horizontal colored band at bottom). This section is focused on the biogeochemical dynamics at the bottom consolidated platelet layer only, being where most of the accumulation of fixed N was observed (Figure 3). It is well known that platelet ice is the most porous of all sea ice types and harbors some of the highest concentrations of sea ice algae (up to $>10,000 \mu\text{g Chl-}a \text{ L}^{-1}$) [*Arrigo et al.*, 1995, 2010]. High exchange rate with seawater (high porosity) and preferential assimilation of N into biomass, trapped within the tortuosity of the brine network, concentrates fixed N in sea ice (Figures 5a and 5c). Preferential assimilation of ^{14}N into biomass, leaving the residual NO_3^- pool enriched in ^{15}N (Figure 5b), and exchange with seawater (brine convection and tidal forcing) preferentially expels ^{15}N out of the sea ice, progressively increasing the concentration of total fixed N and decreasing its $\delta^{15}\text{N}$ [*Fripiat et al.*, 2014], as is observed in the bottom consolidated platelet layer (Figure 4f).

The accumulation of NO_3^- in the bottom consolidated platelet layer, well above the concentration of underlying seawater, has been observed previously in some instances in productive sea ice [*Günther et al.*, 1999; *Riaux-Gobin et al.*, 2000; *Becquevort et al.*, 2009; *Lannuzel et al.*, 2014]. To reach such concentrations, fixed N must be trapped within sea ice. An initial coupling between brine convection and an excess in assimilation over remineralization is able to build a large trapped pool of organic N (several hundred $\mu\text{mol L}^{-1}$; Figures 5a and 5c; presumably in September in this study). Over time, the progressive bacterial colonization, combined with algal mortality, cell lysis and sloppy feeding, liberate organic matter and promote remineralization [*Günther et al.*, 1999; *Thomas and Dieckmann*, 2002; *Meiners et al.*, 2004; *Deming*, 2010], including nitrification [*Fripiat et al.*, 2014]. The resulting transformation of such high concentrations of organic N into NH_4^+ , NO_2^- , and NO_3^- can explain the dissolved N concentrations well above seawater values (Figures 5a and 5d). At this stage, remineralization could be in excess of N assimilation or a tight balance between remineralization and N assimilation could be maintained for a given period of time (October in this study), as long as the environmental conditions are relatively stable. An imbalance toward more N assimilation than remineralization at this stage is not possible, since it would deplete the NO_3^- pool. We believe that brine convection, resulting from a vertical instability in the brine density distribution when ice is growing (Figure 1b), was still ongoing at the bottom of the ice in October. Much higher dissolved inorganic fixed N concentration than that of seawater could be maintained as long as remineralization was a dominant process, outpacing brine convection.

Unexpectedly, the nitrate accumulation in the bottom consolidated platelet layer in October occurred with a high $\text{NO}_3^- \delta^{15}\text{N}$ (12.3–15.2‰; Figure 5b). Much greater NO_3^- production (remineralization + nitrification) than consumption (NO_3^- assimilation) should set the $\text{NO}_3^- \delta^{15}\text{N}$ to a value intermediate between newly produced $\text{NO}_3^- \delta^{15}\text{N}$ (i.e., from nitrification) and seawater $\text{NO}_3^- \delta^{15}\text{N}$ (5.1‰) supplied through brine convection. In the following, we use the current knowledge of N isotope systematic to constrain the relative rates of NO_3^- production and consumption.

Field and laboratory studies suggest that both bacteria and zooplankton preferentially degrade low- $\delta^{15}\text{N}$ PN to ammonium, with a net isotope effect of ~ 2 –5‰ [e.g., *Knapp et al.*, 2011; *Möbius*, 2013, and reference therein]. Ammonium oxidation (AmO, O for oxidation) by marine nitrifiers fractionates the N isotopes, with an isotope effect between 12 and 19‰ [*Casciotti et al.*, 2003]. In the production of regenerated nitrate (nitrification), this fractionation is paired with the subsequent oxidation of nitrite (NiO, Ni for nitrite), which has the rare characteristic of having an inverse isotope effect, with ^{15}N -nitrite being preferentially oxidized (-13 ‰) [*Casciotti*, 2009]. As described above, NO_3^- assimilation (NaU, U for the uptake and Na for nitrate) typically has an isotope effect between 4 and 10‰ [*DiFiore et al.*, 2010]. A large and variable isotope effect has been estimated for NH_4^+ assimilation (AmU), from ~ 5 to 22‰ [*Ivo et al.*, 2013, and references therein]. Its magnitude is dependent on the external ammonia (NH_3) concentration, which controls whether

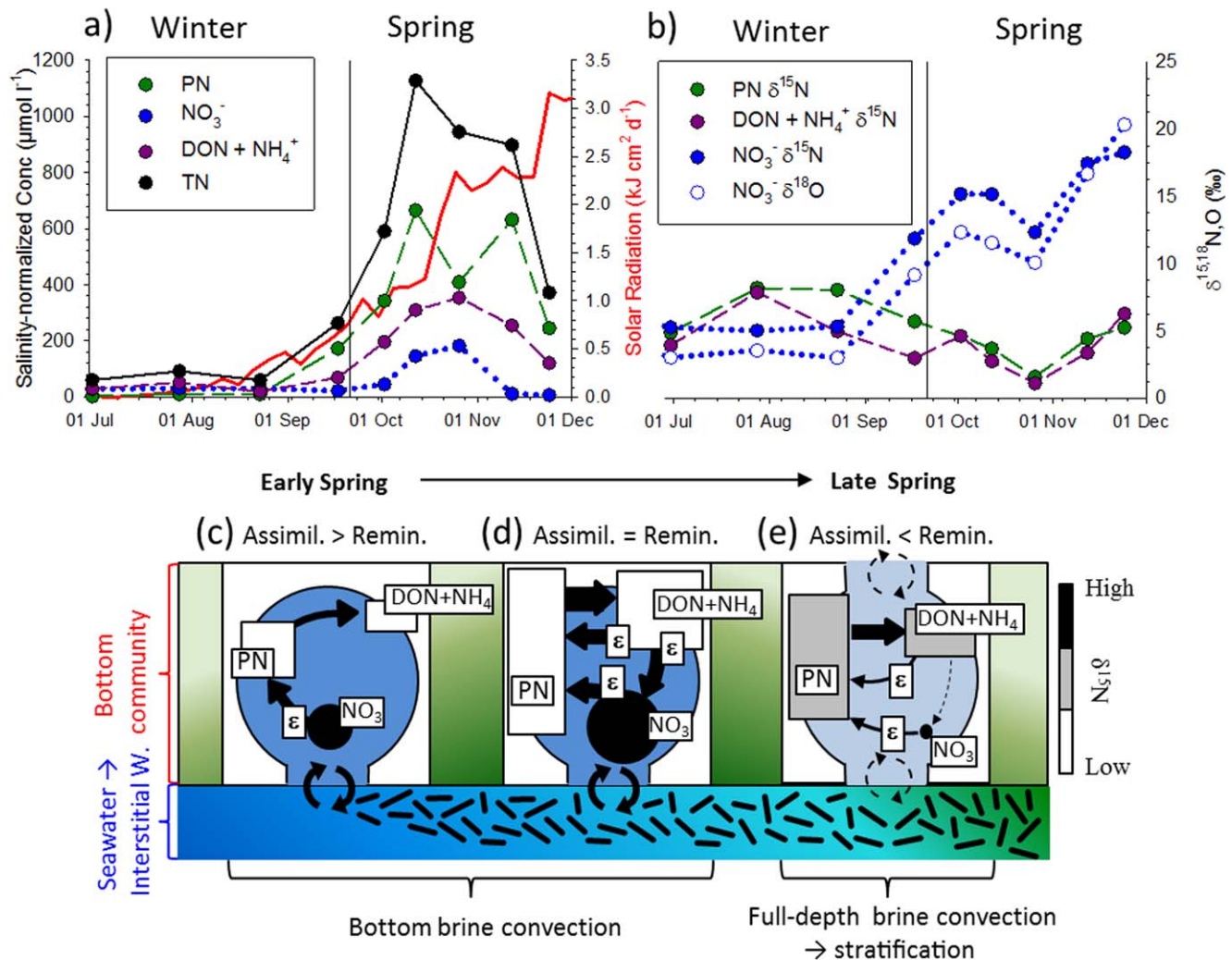


Figure 5. Temporal evolution of salinity-normalized concentration (a) of the fixed N at the bottom of the consolidated ice, together with solar radiation ($\text{kJ cm}^{-2} \text{d}^{-1}$; 5 day average), and (b) associated $\delta^{15}\text{N}$ and $\delta^{18}\text{O}$. (c–e) Conceptual scheme showing the spring nitrogen biogeochemical dynamics at the bottom consolidated platelet layer. The large circles in Figures 5c–5e illustrate brine inclusions with their relative blue scale proportional to salinity (lighter blue = less saline). The relative green scale is proportional to biomass, showing a peak in mid-spring for the bottom consolidated platelet layer and an accumulation in late spring for the loose platelet layer below. The N pools are indicated within the brine inclusions, with their grayscale shade increasing with their $\delta^{15}\text{N}$ and their shape indicating whether they are mobile (circle) or partly immobile (rectangle) [Thomas and Dieckmann, 2002; Meiners et al., 2004; Deming, 2010; Müller et al., 2013]. The arrows linking the N pools reflect biological fluxes, with thicker arrows qualitatively indicating greater fluxes, and an “epsilon” label indicating that the isotopic observations are particularly affected by isotope fractionation at the labeled step. The size of the pool symbol is proportional to the size (concentration) of the pool. The N exchange with seawater (i.e., brine convection and tidal forcing), when combined with nitrate assimilation, caused fixed N to accumulate in the ice (c), from ~ 60 to $1200 \mu\text{mol L}^{-1}$. With the development of an efficient microbial foodweb (bacterial colonization of the organic detritus trapped in the ice), including nitrifiers, the system quickly evolved from new to nearly 100% regenerated production (d). In November, brine volume fraction increased, allowing brine convection through the full thickness of the ice (due to a brine density greater than seawater). This process decreased brine salinity, resulting in vertical stratification within the brine network and, therefore, limiting exchange of fixed N with seawater, resulting in net consumption of the nitrate pool and a likely decay of the sea ice algal bloom (e).

transport across the cell membrane is dominantly active or passive (i.e., diffusive). NH_3 concentration is dependent on the equilibrium constants, NH_4^+ concentration, and pH [Bange, 2007]. Delille et al. [2007] reported a pH range in the brine at Dumont d’Urville between 8.2 and 9.4. In October, brine NH_4^+ concentration was up to $159 \mu\text{mol L}^{-1}$ (brine concentration = bulk SI concentration/brine volume). Using a pK_a of ~ 10.0 for seawater at 0°C , the NH_3 concentration should be above $0.8 \mu\text{mol L}^{-1}$. At such concentrations, an AmU isotope effect of $\sim 22\%$ has been observed, instead of $\sim 5\%$ for lower NH_3 concentration [Vo et al., 2013]. A low-amplitude isotope effect for nitrite assimilation (NiU) has been measured (less than 1%) [Waser et al., 1998].

We simulate three scenarios for the bottom consolidated platelet layer in October (Figure 6). For all of them, there is a balance between the production and consumption processes for both NH_4^+ and NO_2^- . In case (a), inorganic fixed N is produced by the remineralization of organic N and concomitant nitrification, with little

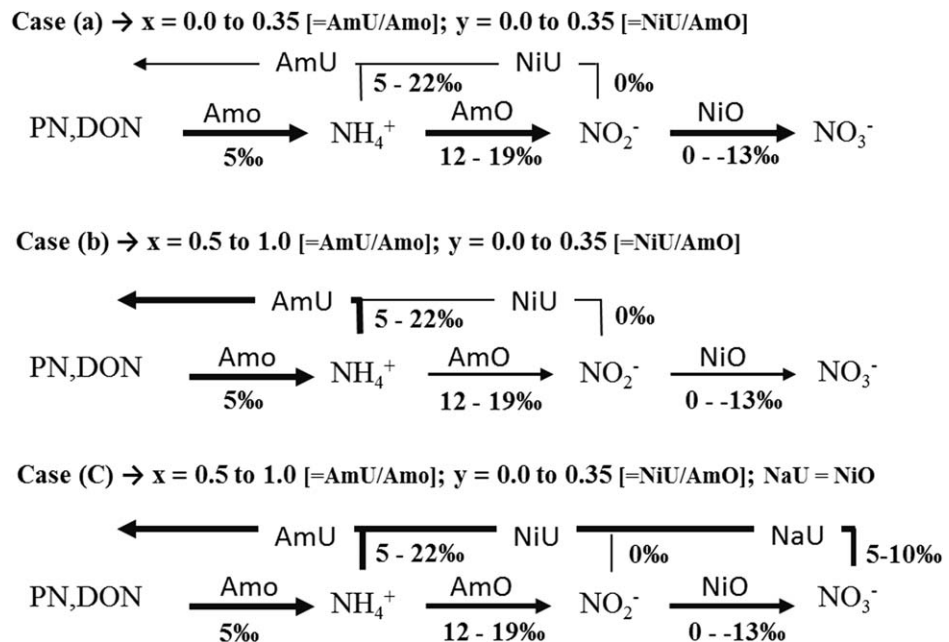


Figure 6. Three scenarios to explain the large accumulation of fixed N at the bottom consolidated platelet community in October. In case (a), there is no significant N assimilation. In case (b), there is significant NH_4^+ assimilation but no significant NO_3^- or NO_2^- assimilation. In case (c), there is significant NH_4^+ assimilation, no significant NO_2^- assimilation, and a balance between NO_2^- oxidation (NiO) and NO_3^- assimilation (NaU). The value or range of values for each isotope effect is taken from the literature [Waser et al., 1998; Casciotti et al., 2003; Casciotti, 2009; Sigman et al., 2009a; DiFiore et al., 2010; Vo et al., 2013, and references therein]. The arrows among the N pools reflect biological fluxes, with thicker arrows qualitatively indicating greater fluxes. The x and y ratios are ratios of NH_4^+ assimilation (AmU)/ammonification (Amo) and NO_2^- assimilation (NiU)/ NH_4^+ oxidation (AmO), respectively. For every case, there is a balance between production and consumption processes for both NH_4^+ and NO_2^- . In cases (b) and (c), a balance also exists for PN + DON.

NH_4^+ and NO_3^- assimilation (Figure 6a); this is a purely heterotrophic system. In alternative case (b), NO_3^- is mainly accumulated but NH_4^+ is actively assimilated, supporting regenerated NH_4^+ -based primary production (Figure 6b). In case (c), a balance between nitrate production and consumption processes is assumed (Figure 6c), such that the rate of nitrification equals that of NO_3^- assimilation. In all cases, we assume that NO_2^- is mainly oxidized into NO_3^- instead of being assimilated. This is in agreement with the current data set in the Southern Ocean [Olson, 1981], suggesting a median contribution of NO_2^- assimilation to the NO_2^- removal of only 2%, with 35% being the highest observed. This is further supported by the small contribution of NO_2^- to the inorganic fixed N pool (median contribution for the bottom consolidated platelet layer is 0.8%).

In the cases (a) and (b), organic N represents by far the dominant N form, imposing its isotopic composition, inherited from previous organic N production, on its release of N. The $\delta^{15}\text{N}$ of ammonium and its products (NO_2^- and NO_3^-) will depend on the combination of isotope effects, the relative importance of which are weighted by the relative contribution of their fluxes to NH_4^+ and NO_2^- removal, as follows (where x and y are AmU/Amo and NiU/AmO, respectively) [Fripiat et al., 2014]:

$$\delta^{15}\text{N}_{\text{NH}_4^+} = \delta^{15}\text{N}_{\text{org.N}} - \epsilon_{\text{Amo}} + x \cdot (\epsilon_{\text{AmU}} - \epsilon_{\text{AmO}}) + \epsilon_{\text{AmO}} \quad (1)$$

$$\delta^{15}\text{N}_{\text{NO}_2^-} = \delta^{15}\text{N}_{\text{org.N}} - \epsilon_{\text{Amo}} + x \cdot (\epsilon_{\text{AmU}} - \epsilon_{\text{AmO}}) + y \cdot (\epsilon_{\text{NiU}} - \epsilon_{\text{NiO}}) + \epsilon_{\text{NiO}} \quad (2)$$

$$\delta^{15}\text{N}_{\text{NO}_3^-} = \delta^{15}\text{N}_{\text{org.N}} - \epsilon_{\text{Amo}} + x \cdot (\epsilon_{\text{AmU}} - \epsilon_{\text{AmO}}) + y \cdot (\epsilon_{\text{NiU}} - \epsilon_{\text{NiO}}) \quad (3)$$

In the alternative case (c) of a balance between nitrification and NO_3^- assimilation (Figure 6c), the $\delta^{15}\text{N}$ of the different fixed N species can be described as follows (equations (1) and (2) are still valid for NH_4^+ and NO_2^-):

$$\delta^{15}\text{N}_{\text{NO}_3^-} = \delta^{15}\text{N}_{\text{org.N}} - \epsilon_{\text{Amo}} + x \cdot (\epsilon_{\text{AmU}} - \epsilon_{\text{AmO}}) + y \cdot (\epsilon_{\text{NiU}} - \epsilon_{\text{NiO}}) + \epsilon_{\text{NaU}} \quad (4)$$

$$\delta^{15}\text{N}_{\text{PN}} = x \cdot (\delta^{15}\text{N}_{\text{NH}_4^+ - \varepsilon_{\text{AmU}}) + y \cdot (1-x) \cdot (\delta^{15}\text{N}_{\text{NO}_2^- - \varepsilon_{\text{NiU}}) + (1-y) \cdot (1-x) \cdot (\delta^{15}\text{N}_{\text{NO}_3^- - \varepsilon_{\text{NaU}}) + \varepsilon_{\text{AmO}} \quad (5)$$

It is generally assumed that, in a productive system, a larger fraction of the ammonium produced by ammonification is assimilated rather than oxidized (i.e., the x ratio is greater than 0.5). The energy yield of ammonium oxidation is low [Ward, 2007], and nitrifiers generally should not be able to out-compete sea ice algae for the available stock of ammonium, the preferred inorganic nitrogen source for assimilation. In cases (b) and (c) for which we assume autotrophic growth, the AmU/AmO ratio (x) is set greater than 0.5 [e.g., Olson, 1981; Bianchi et al., 1997], keeping NiU/AmO ratio (y) lower than 0.35 [Olson, 1981] (the maximum observed in their Southern Ocean study).

In case (a), using all combinations of x and y ratios between 0 and 0.35, assuming organic N at 3‰ and the range for the isotope effects given in Figure 6, the computed $\text{NO}_3^- \delta^{15}\text{N}$ lies between -2.0 and 5.6 ‰ (equation (3)). This is well below the observations within the bottom consolidated platelet layer (Figure 5b), precluding this scenario. $\text{NO}_3^- \delta^{15}\text{N}$ was more than ~ 10 ‰ higher (12.3 – 15.2 ‰), and also higher than seawater $\text{NO}_3^- \delta^{15}\text{N}$ (~ 5.1 ‰). This implies that there was significant N assimilation, increasing the residual $\text{NO}_3^- \delta^{15}\text{N}$, by preferentially channeling ^{14}N into biomass and ^{15}N into inorganic N. In the case (b) of significant NH_4^+ assimilation (x ratio higher than 0.5), but with insignificant NO_3^- assimilation, $\text{NO}_3^- \delta^{15}\text{N}$ ranges from -16 to 12.5 ‰ (equation (3)), still below the observations (12.3 – 15.2 ‰). $\text{NO}_3^- \delta^{15}\text{N}$ is highly dependent of the isotope effect for NH_4^+ assimilation, preferentially channeling ^{14}N into biomass (5 – 22 ‰) [DiFiore et al., 2009; Vo et al., 2013]. As described above, its magnitude is dependent on how $\text{NH}_4^+/\text{NH}_3$ is exchanged in and out the cells [Vo et al., 2013]. High measured/inferred $\text{NH}_4^+/\text{NH}_3$ concentrations should favor the upper range for the isotope effect (22 ‰), which results largely from high amplitude of the equilibrium isotope effect for the dissociation of NH_4^+ to NH_3 [Vo et al., 2013]. With an isotope effect of 22 ‰ the lower limit of the computed $\text{NO}_3^- \delta^{15}\text{N}$ range is revised upward, from -1.1 to 12.5 ‰ (equation (3)), but still below the measured $\text{NO}_3^- \delta^{15}\text{N}$. In case (c), with NaU ranging between 5 and 10 ‰, there is a fit between the computed range and the observations, -11 to 22.6 ‰ (6 – 22.6 ‰ with the isotope effect for NH_4^+ assimilation at 22 ‰; equation (4)) and 12.3 – 15.2 ‰, respectively. By taking the upper range of the field-based isotope effect for NO_3^- assimilation (10 ‰) [DiFiore et al., 2010], the computed range (11 – 22.6 ‰ with the isotope effect for NH_4^+ assimilation at 22 ‰) fits best with the observations. Nitrogen appears, therefore, to be efficiently recycled through the microbial foodweb, with regenerated N, both NH_4^+ and NO_3^- , supporting primary production (Figure 5d). Furthermore, brine convection will supply $\text{NO}_3^- \delta^{15}\text{N}$ at ~ 5.1 ‰ (i.e., underlying seawater). The $\text{NO}_3^- \delta^{15}\text{N}$ of the total input (brine convection + nitrification) should lie between newly produced (i.e., nitrification) and seawater $\text{NO}_3^- \delta^{15}\text{N}$. Thus, if convection also supplied some nitrate, the argument for case (c) (i.e., substantial NO_3^- assimilation) is even stronger.

This scenario (case (c)) is further supported by the $\text{NO}_3^- \delta^{18}\text{O}$ in the bottom consolidated platelet layer in October, which is observed to be higher (10.1 – 12.3 ‰) than in the underlying seawater (2.4 ± 0.3 ‰; Figure 5b). Phytoplankton discriminate against ^{15}N and ^{18}O to a similar extent ($^{15}\varepsilon \sim ^{18}\varepsilon$) [Granger et al., 2004, 2010; Karsh et al., 2012]. As assimilation proceeds, the residual $\text{NO}_3^- \delta^{15}\text{N}$ and $\delta^{18}\text{O}$ should rise nearly equally. In contrast, nitrification affects the nitrate N from O isotopes differently [Lehmann et al., 2004; Sigman et al., 2005]. During NO_3^- assimilation and regeneration, the N isotopes are recycled between the fixed N pools, while the O isotopes are removed in nitrate assimilation (since NO_3^- is reduced to NH_4^+ before assimilation) and then replaced in the nitrification process (NH_4^+ to NO_2^- and then NO_3^-). A field estimate of newly produced $\text{NO}_3^- \delta^{18}\text{O}$ suggests a value close to the ambient $\text{H}_2\text{O} \delta^{18}\text{O} + 1.1$ ‰ [Sigman et al., 2009b]. Coculture experiments (combining NH_4^+ oxidizing Bacteria, NH_4^+ oxidizing Archaea, and NO_2^- oxidizing Bacteria) give a range for the newly produced $\text{NO}_3^- \delta^{18}\text{O}$ between -1.5 and 1.3 ‰ relative to seawater $\text{H}_2\text{O} \delta^{18}\text{O}$ [Buchwald et al., 2012]. Despite some uncertainty in the $\delta^{18}\text{O}$ of newly nitrified nitrate, if the ambient NO_3^- pool was mainly recycled through nitrification, as suggested from the much higher NO_3^- concentration than that of seawater, then the ambient $\text{NO}_3^- \delta^{18}\text{O}$ being produced should be relatively close to the $\text{H}_2\text{O} \delta^{18}\text{O}$. Nitrate exchanges with the underlying seawater should set the $\text{NO}_3^- \delta^{18}\text{O}$ between newly produced nitrate (-1.5 to 1.3 ‰) and seawater nitrate (~ 2.4 ‰). Thus, the observed high $\text{NO}_3^- \delta^{18}\text{O}$ (10.1 – 12.3 ‰ versus VSMOW) again suggests a balance between NO_3^- production (i.e., nitrification; decreasing both $\delta^{15}\text{N}$ and $\delta^{18}\text{O}$) and consumption (i.e., NO_3^- assimilation; increasing both $\delta^{15}\text{N}$ and $\delta^{18}\text{O}$), as follows:

$$\delta^{18}\text{O}_{\text{NO}_3^-} = \delta^{18}\text{O}_{\text{nitrification}} + \varepsilon_{\text{NaU}} \quad (6)$$

Such a balance implies the full environmental expression of the isotope effect. In our calculations, we assume that the $\delta^{18}\text{O}$ of newly produced NO_3^- ($\delta^{18}\text{O}_{\text{nitrification}}$) equals the $\delta^{18}\text{O}$ of ambient H_2O $\delta^{18}\text{O}$ ($\sim 0\text{‰}$) plus 1.1‰ . To produce the observed NO_3^- $\delta^{18}\text{O}$ of $10.1\text{--}12.3\text{‰}$, the isotope effect associated with NO_3^- assimilation must be in the upper range of the field-based isotope effect ($4\text{--}10\text{‰}$) [DiFiore *et al.*, 2010], in agreement with our NO_3^- $\delta^{15}\text{N}$ computation described above (equation (5)).

DiFiore *et al.* [2010] observed a strong correlation between mixed layer depth and field-based isotope effect in the Southern Ocean. Based on this result and previous work [e.g., Needoba and Harrison, 2004], the authors suggested that the variation in ε_{NaU} is driven by the degree of light limitation. The isotope effect associated with NO_3^- assimilation is thought to derive primarily from the rate-limiting NO_3^- reduction to NO_2^- , associated with the enzyme nitrate reductase located in the cytoplasm [Granger *et al.*, 2004, 2010; Karsh *et al.*, 2012]. A greater degree of nitrate efflux allows the intracellular fractionation to be more fully expressed at the organism scale [Needoba *et al.*, 2004]. Needoba *et al.* [2004] suggested that, under light limitation, nitrate uptake is increased relative to the nitrate reduction rate, leading to a larger internal nitrate pool and a much greater fraction of imported nitrate effluxing back into the external medium, increasing the organism-level isotope effect of assimilation. Taking into account the ice conditions in October (Figure 1b) and the light attenuation coefficient for both snow and sea ice ($6\text{--}80\text{ m}^{-1}$ and $0.8\text{--}1.5\text{ m}^{-1}$, respectively) [Nicolaus *et al.*, 2010; Järvinen and Leppäranta, 2011], we calculate that the algae growing in the bottom of the ice received less than a few percent of the surface solar irradiance. This low light level can explain, therefore, why our estimate for the isotope effect ($\sim 10\text{‰}$) is in the upper range of the field-based isotope effects.

To conclude, it seems that the commonly observed high primary production in sea ice returns mainly to the dissolved inorganic pool, through remineralization and nitrification (Figure 5d). Together with the high fixed N concentration (up to 20 times higher than in seawater), the balance between production and consumption processes (i.e., nitrification \approx NO_3^- assimilation) implies that the microbial foodweb is able to process a large amount of fixed N at high rates. This is in agreement with Guglielmo *et al.* [2000], who found rapid turnover rate of the large protein pool by bacterial enzymatic activity in sea ice, as well as with observations of high fixed N assimilation rates [Harrison *et al.*, 1990]. The high N and O isotope effects for nitrate assimilation independently implied by both the $\delta^{15}\text{N}$ and the $\delta^{18}\text{O}$ of nitrate suggest that light limitation of algal growth was important at the base of the ice over this early spring period.

4.3. Spring Evolution to Near-Complete NO_3^- Depletion

With increasing temperature and incoming solar radiation in spring (further increased by the removal of the snow layer; Figure 1b), both primary production and porosity increased throughout the entire ice thickness (Figure 2), allowing full-depth nitrate assimilation and brine convection (Figures 3) [Jardon *et al.*, 2013; Griewank and Notz, 2013]. Together with ice melting, these processes decrease brine salinity (Figure 2b), resulting in a transition to vertical density stratification within the brine network and limiting the subsequent exchange of fixed N with underlying seawater [Tison *et al.*, 2008]. Concomitant with this sequence of events, NO_3^- was removed from the whole ice thickness, from ~ 27 down to $\sim 4\text{ }\mu\text{mol L}^{-1}$, and PN accumulated at the surface and interior of the ice, from ~ 10 to $\sim 30\text{ }\mu\text{mol L}^{-1}$, approximately balancing the NO_3^- depletion (Figure 3). In the bottom of the ice, this succession of events (from convection to stratification) likely promoted the decline of the earlier spring algal bloom (Figure 5e), with a decrease in organic N concentration (Figure 5a). We suggest that the large accumulation in NO_3^- , NH_4^+ , and DON previously observed in October in the bottom consolidated platelet layer was expelled out of sea ice through the full-depth brine convection and replaced by intruding seawater (Figure 3). An increase in light due to the removal of the snow layer in November (Figure 1b) and the decrease in NH_4^+ concentration may have promoted the relative decline of the nitrifier community [e.g., Ward, 2007], preventing a new accumulation of nitrate comparable to that observed in October.

In agreement with the preferential assimilation of ^{14}N and ^{16}O -nitrate, NO_3^- $\delta^{15}\text{N}$ and $\delta^{18}\text{O}$ increased along with NO_3^- depletion (Figures 4a and 4b). In systems without nitrification or other inputs of nitrate during the period of nitrate consumption, the slope given by the relationship between $\text{Ln}(\text{NO}_3^-)$ and both NO_3^- $\delta^{15}\text{N}$ and $\delta^{18}\text{O}$ provides estimates of the net N and O isotope effects associated with NO_3^- consumption (i.e., assuming Rayleigh fractionation) [Sigman *et al.*, 1999]. In order to estimate the net isotope effects as a

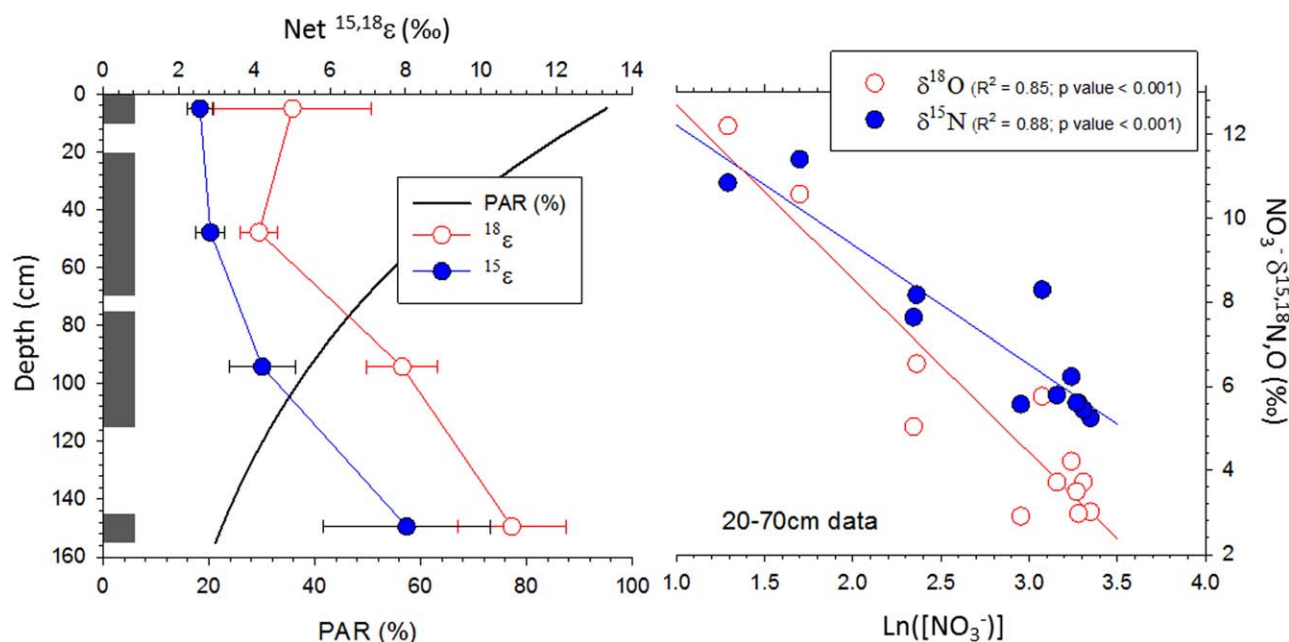


Figure 7. (a) Estimates of “net” N and O isotope effects for nitrate assimilation with depth, (b) with an example (using the 20–70 cm depth layer) of how they are calculated. The net isotope effect is estimated by the slope of the relationship between $\text{Ln}(\text{NO}_3^-)$ and either the $\delta^{15}\text{N}$ or $\delta^{18}\text{O}$ of NO_3^- (b), assuming Rayleigh fractionation kinetics [Sigman *et al.*, 1999]. The black line in Figure 7a represents the percentage of the incident photosynthetically active radiation with depth, assuming a light attenuation coefficient of 1.0 m^{-1} for natural sea ice [Nicolaus *et al.*, 2010]. The gray bars in Figure 7a represent the depth range for which the data have been taken to estimate the isotope effects. In the text, it is explained that nitrification has likely affected these isotope effect estimates but cannot explain their increase with depth.

function of depth, NO_3^- concentration and $\delta^{15}\text{N}$ from June to November have been binned by depth (0–10, 20–70, 75–115, and 145–155 cm; Figure 7a). For the bottom ice section, (i) we excluded from this calculation the observations with NO_3^- concentration higher than in seawater, as this indicates violation of the Rayleigh criteria (bottom section in October; section 5.2), and (ii) we took the average underlying seawater as initial conditions since no ice was present at this depth before October. The isotope effects estimated in this way decreased upward through the ice (Figure 7), with lower values for N than O isotopes ($R^2 > 0.77$, except for the surface $^{18}\epsilon$ estimate with $R^2 = 0.46$). Assuming a light attenuation coefficient for natural sea ice between 0.8 and 1.5 m^{-1} [Nicolaus *et al.*, 2010] and the ice conditions in November (no snow cover and an ice thickness averaging 152 cm; Figure 1b), the percentage of photosynthetically active radiation (PAR) decreased downward (Figure 7a) and was anticorrelated with the net N and O isotope effects. Consistent with the findings of the previous section, we hypothesize that this correlation is driven by the degree of light limitation [Needoba *et al.*, 2004; DiFiore *et al.*, 2010], with higher cellular efflux of nitrate and leading to higher N and O isotope effects in the deeper ice.

However, the discrepancy between the O and N isotope effects suggests a different or complementary interpretation for the variations in the Rayleigh-based estimates. $\Delta(15-18)$ is a metric that has been proposed to assess the decoupling between N and O isotopes ($\Delta(15-18) = \text{NO}_3^- \delta^{15}\text{N} - \text{NO}_3^- \delta^{18}\text{O}$) [Rafter *et al.*, 2013]. With only NO_3^- assimilation, $\Delta(15-18)$ should remain unchanged (initial $\Delta(15-18)$ of $2.6 \pm 0.3\text{‰}$, taken from the average underlying seawater nitrate). In the sea ice system studied here, nitrification decreases the $\Delta(15-18)$ by regenerating nitrate that is much lower than ambient nitrate in $\delta^{15}\text{N}$ but only modestly lower in $\delta^{18}\text{O}$ [Sigman *et al.*, 2005, 2009b]. Low $\Delta(15-18)$ was observed throughout the entire ice thickness in November (Figure 4c), relative to seawater. The lowest $\Delta(15-18)$ (reaching -9‰) was observed in the interior of the ice just above the ice bottom. Such decoupling indicates that nitrification was ongoing throughout the entire ice thickness in November, and can explain the lower apparent isotope effect of nitrate assimilation for N than O (Figure 7a). In addition, nitrification decreases the estimate of the net isotope effect associated with NO_3^- consumption, by regenerating nitrate bearing a lower $\delta^{15}\text{N}$ and $\delta^{18}\text{O}$ than that of the ambient nitrate; thus, these estimates for the isotope effects of nitrate assimilation (Figure 7) should be taken as lower bounds. However, nitrification alone is not able to explain the relationship between net isotope effect estimates and depth (Figure 7a): nitrification should have artificially lowered the

deep isotope effect estimates relative to the shallow estimates, but the observation is of increasing isotope effects with depth (Figure 7a). To summarize, it appears that both nitrification and light limitation of nitrate assimilation affect the nitrate isotopes within landfast sea ice in the spring.

5. Conclusions

This study reports on the temporal evolution, from April to November, in the concentration of the main fixed N forms (particulate N, dissolved organic N, ammonium, nitrite, and nitrate) and their isotopic compositions ($\delta^{15}\text{N}$ of PN, dissolved organic N + ammonium, and nitrate; $\delta^{18}\text{O}$ of nitrate) in Antarctic landfast sea ice, in the vicinity of the French station "Dumont d'Urville." Antarctic landfast sea ice is one of the most productive environments on Earth and worthy of study for this and other reasons.

Combined with N concentration measurements, N and O isotope distributions unravel the dominant processes affecting sea ice fixed N. In autumn when seawater freezes, microorganisms incorporated into the sea ice matrix are actively growing, depleting nitrate and accumulating organic N. No major changes are observed in winter, suggesting that environmental conditions (low light, low temperature and high salinity) impose low biological activity in the dominantly closed brine structures. During early spring in the consolidated platelet layer at the bottom of the ice, fixed N is accumulated at high rates (yielding concentrations up to $1200 \mu\text{mol L}^{-1}$, salinity-normalized). The only way to accumulate this amount of fixed N (mainly organic) is to couple nutrient supply from the underlying seawater through brine convection with assimilation into immobile biomass that becomes trapped within the tortuosity of the brine network. The subsequent colonization of this organic matter by an efficient microbial foodweb remineralizes and nitrifies fixed N at high rates, with normalized nitrate concentrations up to $\sim 200 \mu\text{mol L}^{-1}$. However, nitrate $\delta^{15}\text{N}$ and $\delta^{18}\text{O}$ in the consolidated platelet layer remain higher than expected from nitrification alone. This difference indicates a balance between N assimilation and remineralization, with the rate of nitrification nearly equaling that of nitrate assimilation. Thus, the primary production at this time is fueled largely by regenerated N. When sea ice warm in spring and the brine network stratifies, sea ice algae deplete nitrate through the full thickness of the ice. The extent of the isotope fractionation associated with nitrate assimilation appears to be affected by light availability [Needoba et al., 2004; DiFiore et al., 2010]. Thus, isotope data suggest that light is a scarce resource in landfast sea ice, especially in the bottom ice section where most the biomass accumulation occurs. In addition, the O-to-N isotope relationship of nitrate indicates that nitrification is active even during this period of net nitrate consumption.

Acknowledgments

Data are available as in supporting information Table S1. Our warm thanks go to the crews of the French station "Dumont d'Urville" and to the French Polar Institute (IPEV) for the logistic supports through the ICELIPIDS project (project 1010; lead by G. Massé). We are also grateful to C. Robineau for the sampling; to M. A. Weigand and S. Oleynik for the management of the GC-IRMS laboratory at Princeton University; and to S. El Amri for her help in the management of the glaciology unit of ULB. This research was supported by the Belgian Science policy (BIGSOUTH network, SD/CA/05A of SPSDIII, Support Plan for Sustainable Development), the U.S. NSF through grants OPP-0453680, OPP-0612198, OCE-0992345-, and PLR-1401489, and by the Grand Challenges Program at Princeton University. François Fripiat was and is a postdoctoral fellow with the "Fonds National de la Recherche Scientifique" (FNRS, Belgium) and "Fonds Wetenschappelijk Onderzoek" (FWO, Belgium).

References

- Arrigo, K. R., and D. N. Thomas (2004), Large scale importance of sea ice biology in the Southern Ocean, *Antarct. Sci.*, *16*(4), 471–486.
- Arrigo, K. R., G. Dieckmann, M. Gosselin, D. H. Robinson, C. H. Fritsen, and C. W. Sullivan (1995), High resolution study of the platelet ice ecosystem in McMurdo Sound, Antarctica: Biomass, nutrient, and production profiles within a dense microalgal bloom, *Mar. Ecol. Prog. Ser.*, *127*, 255–268.
- Arrigo, K. R., T. Mock, and M. P. Lizotte (2010), Primary producers and sea ice, in *Sea Ice*, edited by D. N. Thomas and G. S. Dieckmann, pp. 283–325, Blackwell Sci., Oxford, U. K.
- Bange, H. W. (2007), Gaseous nitrogen compounds (NO , N_2O , N_2 , NH_3) in the ocean, in *Nitrogen in the Marine Environment*, edited by D. G. Capone et al., pp. 51–94, Elsevier, Amsterdam.
- Becquevort, S., I. Dumont, J.-L. Tison, D. Lannuzel, M.-L. Sauvée, L. Chou, and V. Schoemann (2009), Biogeochemistry and microbial community composition in sea ice and underlying seawater off East Antarctica during early spring, *Polar Biol.*, *32*, 879–895.
- Bianchi, M., F. Feliatra, P. Tréguer, M.-A. Vincendeau, and J. Morvan (1997), Nitrification rates, ammonium and nitrate distribution in upper layers of the water column and in sediments of the Indian sector of the Southern Ocean, *Deep Sea Res., Part II*, *44*(5), 1017–1032.
- Böhlke, J. K., S. J. Mroczkowski, and T. B. Coplen (2003), Oxygen isotope in nitrate: New reference materials for ^{18}O : ^{17}O : ^{16}O measurements and observations on nitrate-water equilibration, *Rapid Commun. Mass Spectrom.*, *17*, 1835–1846.
- Braman, R. S., and S. A. Hendrix (1989), Nanogram nitrite and nitrate determination in environmental and biological materials by vanadium(III) reduction with chemiluminescence detection, *Anal. Chem.*, *61*, 2715–2718.
- Buchwald, C., A. E. Santoro, M. R. McIlvin, and K. L. Casciotti (2012), Oxygen isotopic composition of nitrate and nitrite produced by nitrifying cocultures and natural marine assemblages, *Limnol. Oceanogr.*, *57*(5), 1361–1375.
- Casciotti, K. L. (2009), Inverse kinetic isotope fractionation during bacterial nitrite oxidation, *Geochim. Cosmochim. Acta*, *73*, 2061–2076.
- Casciotti, K. L., D. M. Sigman, M. G. Hastings, J. K. Böhlke, and A. Hilkert (2002), Measurement of the oxygen isotopic composition of nitrate in seawater and freshwater using denitrifier method, *Anal. Chem.*, *74*, 4905–4912.
- Casciotti, K. L., D. M. Sigman, and B. B. Ward (2003), Linking diversity and stable isotope fractionation in ammonia-oxidizing bacteria, *Geomicrobiol. J.*, *20*, 335–353.
- Checkley, D. M., and C. A. Miller (1989), Nitrogen isotope fractionation by oceanic zooplankton, *Deep Sea Res., Part A*, *36*(10), 1449–1456.
- Cox, G. F. N., and W. F. Weeks (1983), Equations for determining the gas and brine volumes in sea-ice samples, *J. Glaciol.*, *29*(102), 306–316.
- Delille, B., B. Jourdain, A. V. Borges, J.-L. Tison, and D. Delille (2007), Biogas (CO_2 , O_2 , dimethylsulfide) dynamics in spring Antarctic fast ice, *Limnol. Oceanogr.*, *52*(4), 1367–1379.

- Delille, D. (1990), Factors affecting the horizontal patchiness of Coastal Antarctic Seawater Bacteria, *Polar Biol.*, *11*, 41–45.
- Delille, D., M. Fiala, J. Kuparinen, H. Kuosa, and C. Plessis (2002), Seasonal changes in microbial biomass in the first-year ice of the Terre Adélie area (Antarctica), *Aquat. Microb. Ecol.*, *28*, 257–265.
- Deming, J. W. (2010), Sea ice bacteria and viruses, in *Sea Ice*, edited by D. N. Thomas and G. S. Dieckmann, pp. 247–282, Blackwell Sci., Oxford, U. K.
- Dempsey, D. E., and P. J. Langhorne (2012), Geometric properties of platelet ice crystals, *Cold Reg. Sci. Technol.*, *78*, 1–13.
- Dieckmann, G. S., K. Arrigo, and C. W. Sullivan (1992), A high-resolution sampler for nutrient and chlorophyll a profiles of the sea ice platelet layer and underlying water column below fast ice in polar oceans: Preliminary results, *Mar. Ecol. Prog. Ser.*, *80*, 291–300.
- DiFiore, P. J., D. M. Sigman, T. W. Trull, M. J. Lourey, K. Karsh, G. Cane, and R. Ho (2006), Nitrogen isotope constraints on Subantarctic biogeochemistry, *J. Geophys. Res.*, *111*, C08016, doi:10.1029/2005JC003216.
- DiFiore, P. J., D. M. Sigman, and R. B. Dunbar (2009), Upper ocean nitrogen fluxes in the Polar Antarctic Zone: Constraints from the oxygen and nitrogen isotopes of nitrate, *Geochem. Geophys. Geosyst.*, *10*, Q11016, doi:10.1029/2009GC002468.
- DiFiore, P. J., D. M. Sigman, K. L. Karsh, T. W. Trull, R. B. Dunbar, and R. S. Robinson (2010), Poleward decrease in the isotope effect of nitrate assimilation across the Southern Ocean, *Geophys. Res. Lett.*, *37*, L17601, doi:10.1029/2010GL044090.
- Eicken, H., M. E. Lange, and G. S. Dieckmann (1991), Spatial variability of sea-ice properties in the Northwestern Weddell Sea, *J. Geophys. Res.*, *96*(C6), 10,603–10,615.
- Flores, H., B. P. V. Hunt, S. Kruse, E. A. Pakhomov, V. Siegel, J. A. van Franeker, V. Strass, A. P. Van de Putte, E. H. W. G. Meesters, and U. Bathmann (2014), Seasonal changes in the vertical distribution and community structure of Antarctic macrozooplankton and micronekton, *Deep Sea Res., Part 1*, *84*, 127–141.
- Fraser, A. D., R. A. Massom, K. J. Michael, B. K. Galton-Fenzi, and J. L. Lieser (2012), East Antarctic Landfast Sea Ice distribution and variability, 2000–08, *J. Clim.*, *25*, 1137–1156, doi:10.1175/JCLI-D-10-05032.1.
- Fripiat, F., D. Cardinal, J.-L. Tison, A. Worby, and L. André (2007), Diatom-induced silicon isotopic fractionation in Antarctic sea ice, *J. Geophys. Res.*, *112*, GB02001, doi:10.1029/2006JG000244.
- Fripiat, F., D. M. Sigman, S. E. Fawcett, P. A. Rafter, M. A. Weigand, and J.-L. Tison (2014), New insights into sea ice nitrogen biogeochemical dynamics from the nitrogen isotopes, *Global Biogeochem. Cycles*, *28*, 115–130, doi:10.1002/2013GB004729.
- Galindo, V., M. Levasseur, C. J. Mundy, M. Gosselin, J.-E. Tremblay, M. Scarrat, Y. Gratton, T. Papakiriakou, M. Poulin, and M. Lizotte (2014), Biological and physical processes influencing sea ice, under-ice algae, and dimethylsulfoniopropionate during spring in the Canadian Arctic Archipelago, *J. Geophys. Res. Oceans*, *119*, 3746–3766, doi:10.1002/2013JC009497.
- Garcia, H. E., R. A. Locarnini, T. P. Boyer, and J. I. Antonov (2005), World Ocean Atlas 2005, volume 4: Nutrients (phosphate, nitrate, silicate), edited by: S. Levitus, NOAA Atlas NESDIS 64, 396 pp., U.S. Govern. Print. Off., Washington, D. C.
- Garside, C. (1982), A chemiluminescent technique for the determination of nanomolar concentrations of nitrate and nitrite in seawater, *Mar. Chem.*, *11*, 159–167.
- Gleitz, M., M. R. van der Loeff, D. N. Thomas, G. S. Dieckmann, and F. J. Millero (1995), Comparison of summer and winter inorganic carbon, oxygen and nutrient concentrations in Antarctic sea ice brine, *Mar. Chem.*, *51*, 81–91.
- Golden, K. M., S. F. Ackley, and V. I. Lytle (1998), The percolation phase transition in sea ice, *Science*, *282*, 2238–2241.
- Granger, J., and D. M. Sigman (2009), Removal of nitrite with sulfamic acid for nitrate N and O isotope analysis with the denitrifier method, *Rapid Commun. Mass. Spectrom.*, *23*, 3753–3762.
- Granger, J., D. M. Sigman, J. A. Needoba, and P. J. Harrison (2004), Coupled nitrogen and oxygen isotope fractionation of nitrate during assimilation by cultures of marine phytoplankton, *Limnol. Oceanogr.*, *49*(5), 1763–1773.
- Granger, J., D. M. Sigman, M. M. Rohde, M. T. Maldonado, and P. D. Tortell (2010), N and O isotope effects during nitrate assimilation by unicellular prokaryotic and eukaryotic plankton cultures, *Geochim. Cosmochim. Acta*, *74*, 1030–1040.
- Granger, J., M. G. Prokopenko, C. W. Mordy, and D. M. Sigman (2013), The proportion of remineralized nitrate on the ice-covered eastern Bering Sea shelf evidenced from the oxygen isotope ratio of nitrate, *Global Biogeochem. Cycles*, *27*, 962–971, doi:10.1002/gbc.20075.
- Griewank, P. J., and D. Notz (2013), Insights into brine dynamics and sea ice desalination from a 1-D model study of gravity drainage, *J. Geophys. Res. Oceans*, *118*, 3370–3386, doi:10.1002/jgrc.20247.
- Guglielmo, L., G. C. Carrada, G. Catalano, A. Dell'Anno, M. Fabiano, L. Lazzara, O. Mangoni, A. Pusceddu, and V. Saggiomo (2000), Structural and functional properties of sympagic communities in the annual sea ice at Terra Nova Bay (Ross Sea, Antarctica), *Polar Biol.*, *23*, 137–146.
- Günther, S., M. Gleitz, and G. S. Dieckmann (1999), Biogeochemistry of Antarctic sea ice: A case study on platelet ice layers at Drescher Inlet, Weddell Sea, *Mar. Ecol. Prog. Ser.*, *177*, 1–13.
- Harrison, W. G., G. F. Cota, and R. E. H. Smith (1990), Nitrogen utilization in ice algal communities of Barrow Strait, Northwest Territories, Canada, *Mar. Ecol. Prog. Ser.*, *67*, 275–283.
- Holmes, R. M., A. Aminot, R. Kérouel, B. A. Hooker, and B. J. Peterson (1999), A simple and precise method of measuring ammonium and marine and freshwater ecosystems, *Can. Data Rep. Fish. Aquat. Sci.*, *56*, 1801–1808.
- Jardon, F. P., F. Vivier, M. Vancoppenolle, A. Lourenço, P. Bouruet-Aubertot, and Y. Cuypers (2013), Full-depth desalination of warm sea ice, *J. Geophys. Res. Oceans*, *118*, 435–447, doi:10.1029/2012JC007962.
- Järvinen, O., and M. Leppäranta (2011), Transmission of solar radiation through the snow cover on floating ice, *J. Glaciol.*, *57*(205), 861–870.
- Junge, K., H. Eicken, and J. W. Deming (2004), Bacterial activity at -2 to -20°C in Arctic wintertime sea ice, *Appl. Environ. Microbiol.*, *70*(1), 550–557.
- Karsh, K. L., J. Granger, K. Kritee, and D. M. Sigman (2012), Eukaryotic assimilatory nitrate reductase fractionates N and O isotopes with a ratio near unity, *Environ. Sci. Technol.*, *46*, 5727–5735.
- Knapp, A. N., D. M. Sigman, and F. Lipschultz (2005), N isotopic composition of dissolved organic nitrogen and nitrate at the Bermuda Atlantic Time-series Study site, *Global Biogeochem. Cycles*, *19*, GB1018, doi:10.1029/2004GB002320.
- Knapp, A. N., D. M. Sigman, F. Lipschultz, A. B. Kustka, and D. G. Capone (2011), Interbasin isotopic correspondence between upper-ocean bulk DON and subsurface nitrate and its implications for marine nitrogen cycling, *Global Biogeochem. Cycles*, *25*, GB4004, doi:10.1029/2010GB003878.
- Lancelot, C., A. de Montety, H. Goosse, S. Becquevort, V. Schoemann, B. Pasquer, and M. Vancoppenolle (2009), Spatial distribution of the iron supply to phytoplankton in the Southern Ocean: A model study, *Biogeosciences*, *6*, 2861–2878.
- Lannuzel, D., A. R. Bowie, P. C. van der Merwe, A. T. Townsend, and V. Schoemann (2011), Distribution of dissolved and particulate metals in Antarctic sea ice, *Mar. Chem.*, *124*, 134–146.

- Lannuzel, D., P. C. van der Merwe, A. T. Townsend, and A. Bowie (2014), Size fractionation of iron, manganese and aluminium in Antarctic fast ice reveals a lithogenic origin and low iron solubility, *Mar. Chem.*, *161*, 47–56.
- Lehmann, M. F., D. M. Sigman, and W. M. Berelson (2004), Coupling the $^{15}\text{N}/^{14}\text{N}$ and $^{18}\text{O}/^{16}\text{O}$ of nitrate as a constraint on benthic nitrogen cycling, *Mar. Chem.*, *88*, 1–20.
- Martiny, A. C., J. A. Vrugt, F. W. Primeau, and M. W. Lomas (2013), Regional variation in the particulate organic carbon to nitrogen ratio in the surface ocean, *Global Biogeochem. Cycles*, *27*, 723–731, doi:10.1002/gbc.20061.
- Meiners, K., R. Brinkmeyer, M. A. Granskog, and A. Lindfors (2004), Abundance, size distribution and bacterial colonization of exopolymer particles in Antarctic sea ice (Bellingshausen Sea), *Aquat. Microb. Ecol.*, *35*, 283–296.
- Meiners, K. M., et al. (2012), Chlorophyll a in Antarctic sea ice from historical ice core data, *Geophys. Res. Lett.*, *39*, L21602, doi:10.1029/2012GL0534478.
- Miller, L. A., et al. (2015), Methods for biogeochemical studies of sea ice: The state of the art, caveats, and recommendations, *Elementa Sci. Anthropocene*, *3*, 000038, doi:10/12952/journal.elementa.000038.
- Möbius, J. (2013), Isotope fractionation during nitrogen remineralization (ammonification): Implications for nitrogen isotope biogeochemistry, *Geochim. Cosmochim. Acta*, *105*, 422–432.
- Müller, S., A. V. Vähätalo, C. A. Stedmon, M. A. Granskog, L. Norman, S. N. Aslam, G. J. C. Underwood, G. S. Dieckmann, and D. N. Thomas (2013), Selective incorporation of dissolved organic matter (DOM) during sea ice formation, *Mar. Chem.*, *155*, 148–157.
- Needoba, J. A., and P. J. Harrison (2004), Influence of low light and a light:dark cycle on NO_3^- uptake, intracellular NO_3^- , and nitrogen isotope fractionation by marine phytoplankton, *J. Phycol.*, *40*, 505–516.
- Needoba, J. A., D. M. Sigman, and P. J. Harrison (2004), The mechanism of isotope fractionation during algal nitrate assimilation as illuminated by the $^{15}\text{N}/^{14}\text{N}$ of intracellular nitrate, *J. Phycol.*, *40*, 517–522.
- Nicolaus, M., S. Gerland, S. R. Hudson, S. Hanson, J. Haapala, and D. K. Perovich (2010), Seasonality of spectral albedo and transmissivity as observed in the Arctic Transpolar Drift in 2007, *J. Geophys. Res.*, *115*, C11011, doi:10.1029/JC006074.
- Notz, D., J. S. Wettlaufer, and M. G. Worster (2005), Instruments and methods: A non-destructive method for measuring the salinity and solid fraction of growing sea ice in situ, *J. Glaciol.*, *51*(172), 159–166.
- Olson, R. J. (1981), ^{15}N tracer studies of the primary nitrite maximum, *J. Mar. Res.*, *39*(2), 203–238.
- Petrich, C., P. J. Langhorne, and Z. F. Sun (2006), Modelling the interrelationships between permeability, effective porosity and total porosity in sea ice, *Cold Reg. Sci. Technol.*, *44*, 131–144, doi:10.1016/j.coldregions.2005.10.001.
- Qi, H., T. B. Coplen, H. Geilmann, W. A. Brand, and J. K. Böhlke (2003), Two new organic reference materials for $\delta^{13}\text{C}$ and $\delta^{15}\text{N}$ measurements and a new value for the $\delta^{13}\text{C}$ of NBS22 oil, *Rapid Commun. Mass Spectrom.*, *17*, 2483–2487.
- Rafter, P. A., P. J. DiFiore, and D. M. Sigman (2013), Coupled nitrate nitrogen and oxygen isotopes and organic matter remineralization in the Southern and Pacific oceans, *J. Geophys. Res. Oceans*, *118*, 4781–4794, doi:10.1002/jgrc.20316.
- Riaux-Gobin, C., P. Tréguer, M. Poulin, and G. Vétion (2000), Nutrients, algal biomass and communities in land-fast ice and seawater off Adélie Land (Antarctica), *Antarct. Sci.*, *12*(2), 160–171.
- Riaux-Gobin, C., P. Tréguer, G. Dieckmann, E. Maria, G. Vétion, and M. Poulin (2005), Land-fast ice off Adélie Land (Antarctica): short-term variations in nutrients and chlorophyll just before ice break-up, *J. Mar. Syst.*, *55*, 235–248.
- Rysgaard, S., R. N. Glud, M. K. Sejr, M. E. Blichner, and J. Stahl (2008), Denitrification activity and oxygen dynamics in Arctic sea ice, *Polar Biol.*, *31*, 527–537.
- Rysgaard, S., J. Bendtsen, B. Delille, G. S. Dieckmann, R. N. Glud, H. Kennedy, J. Mortensen, S. Papadimitriou, D. N. Thomas, and J.-L. Tison (2011), Sea ice contribution to the air-sea CO_2 exchange in the Arctic and Southern Oceans, *Tellus, Ser. B*, *63*, 823–830.
- Schlitzer, R. (2015), Ocean Data View. [Available at <http://odv.awi.de>.]
- Sigman, D. M., M. A. Altabet, D. C. McCorkle, R. Francois, and G. Fischer (1999), The $\delta^{15}\text{N}$ of nitrate in the Southern Ocean: Consumption of nitrate in surface waters, *Global Biogeochem. Cycles*, *13*(4), 1149–1166.
- Sigman, D. M., K. L. Casciotti, M. Andreani, C. Barford, M. Galanter, and J. K. Böhlke (2001), A bacterial method for the nitrogen isotopic analysis of nitrate in seawater and freshwater, *Anal. Chem.*, *73*, 4145–4153.
- Sigman, D. M., J. Granger, P. J. DiFiore, M. M. Lehmann, R. Ho, G. Cane, and A. van Green (2005), Coupled nitrogen and oxygen isotope measurements of nitrate along the eastern North Pacific margin, *Global Biogeochem. Cycles*, *19*, GB4022, doi:10.1029/2005GB002458.
- Sigman, D. M., K. L. Karsh, and K. L. Casciotti (2009a), Nitrogen isotopes in the ocean, in *Encyclopedia of Ocean Sciences*, edited by J. H. Steele, K. K. Turekian, and S. A. Thorpe, pp. 4138–4153, Academic, London, U. K. [Update from 2001]
- Sigman, D. M., P. J. DiFiore, M. P. Hain, C. Deutsch, Y. Wang, D. M. Karl, A. N. Knapp, M. F. Lehmann, and S. Pantoja (2009b), The dual isotopes of deep nitrate as a constraint on the cycle and budget of oceanic fixed nitrogen, *Deep Sea Res., Part I*, *56*, 1419–1439.
- Smith, W. O., and D. M. Nelson (1985), Phytoplankton bloom produced by a receding ice edge in the Ross Sea: Spatial coherence with the density field, *Science*, *227*, 163–166.
- Thomas, D. N., and G. S. Dieckmann (2002), Antarctic Sea Ice—A habitat for extremophiles, *Science*, *295*, 641–644.
- Thomas, D. N., G. Kattner, R. Engbrodt, V. Giannelli, H. Kennedy, C. Hass, and G. S. Dieckmann (2001), Dissolved organic matter in Antarctic sea ice, *Ann. Glaciol.*, *33*, 297–303.
- Thomas, D. N., S. Papadimitriou, and C. Michel (2010), Biogeochemistry of sea ice, in *Sea Ice*, edited by D. N. Thomas and G. S. Dieckmann, pp. 425–467, Blackwell Sci., Oxford, U. K.
- Thomas, T. (1986), L'effectif des oiseaux nicheurs de l'archipel de Cape Geology (Terre Adélie) et son évolution au cours des trente dernières années, *L'oiseau RFO*, *56*, 349–368.
- Tison, J.-L., A. Worby, B. Delille, F. Brabant, S. Papadimitriou, D. Thomas, J. de Jong, D. Lannuzel, and C. Haas (2008), Temporal evolution of decaying summer first-year sea ice in the western Weddell Sea, Antarctica, *Deep Sea Res., Part II*, *55*, 975–987.
- Vancoppenolle, M., H. Goosse, A. de Montety, T. Fichefet, B. Tremblay, and J.-L. Tison (2010), Modeling brine and nutrient dynamics in Antarctic sea ice: The case of dissolved silica, *J. Geophys. Res.*, *115*, C02005, doi:10.1029/2009JC005369.
- Vancoppenolle, M., et al. (2013), Role of sea ice in global biogeochemical cycles: Emerging views and challenges, *Quat. Sci. Rev.*, *79*, 207–230.
- Vo, J., W. Inwood, J. M. Hayes, and S. Kustu (2013), Mechanism for nitrogen isotope fractionation during ammonium assimilation by *Escherichia coli* K12, *Proc. Natl. Acad. Sci. U. S. A.*, *110*(21), 8696–8701.
- Wada, E., R. Shibata, and T. Torii (1981), ^{15}N abundance in Antarctica: Origin of soil nitrogen and ecological implications, *Nature*, *292*, 327–329.
- Wankel, S. D., C. Kendall, J. T. Pennington, F. P. Chavez, and A. Paytan (2007), Nitrification in the euphotic zone as evidenced by nitrate dual isotopic composition: Observations from Monterey Bay, California, *Global Biogeochem. Cycles*, *21*, GB2009, doi:10.1029/2006GB002723.

- Ward, B. B. (2007), Nitrification in marine systems, in *Nitrogen in the Marine Environment*, edited by D. G. Capone et al., pp. 199–261, Elsevier, Amsterdam.
- Waser, N. A. D., P. J. Harrison, B. Nielsen, and S. E. Calvert (1998), Nitrogen isotope fractionation during the uptake and assimilation of nitrate, nitrite, ammonium, and urea by a marine diatom, *Limnol. Oceanogr.*, *43*(2), 215–224.
- Weeks, W. F., and S. F. Ackley (1986), The growth, structure, and properties of sea ice, in *The Geophysics of Sea Ice*, NATO ASI Ser. B Phys., vol. 146, edited by N. Untersteiner, pp. 9–164, Plenum, N. Y.